Ecole polytechnique fédérale de Lausanne

Laboratory of ecohydrology

Master Thesis

Modelling spatial patterns in soil Red-Ox cycling under different ecohydrological scenarios

Mosé Roberto Balmelli

Project advisor: Prof. Andrea Rinaldo
Co-advisor: Dr. Filippo Miele

June 2021

EPFL

This project was performed from February 2021 to June 2021 in the Laboratory of ecohydrology ECHO

Abstract

In the soil, different biogeological cycles intertwine, interact and influence each other. Among these, the Dissimilatory Fe^{2+}/Fe^{3+} reduction cycle plays a key role in many biogeochemical process as bioremediation and degradation of organic matter occurring in the soil and it is intimately influenced by ecohydrological conditions.

In order to model the dynamics of the biomass mediated dissimilatory iron reduction under fluctuating saturation's condition it is necessary to use equations that couple both reaction and transport terms.
In a first step, an analytical study of the model proposed by Calabrese and Porporato, which models the time evolution of the redox couple Fe^{2+}/Fe^{3+} in soil as a single bioreactor, will be carried out. After studying the fixed points of the reactive terms and performing an instability analysis of the stationary solutions, the dynamics of Fe^{2+}, Fe^{3+}, carbon substrate and population of Fe-reducers will be simulated under different ecohydrological scenarios.

The model will be then extended to its spatial explicit formulation by hosting the reaction terms in a multi-layered soil framework. Further simulations will be carried out under different ecohydrological conditions to investigate the differences and challenges of the implemented model when coupled to the stochasticity of rainfall events. In a multi-layer soil, substantial differences between the surface layers and the deeper ones occur. Such differences are given by different hydrological inputs and more realistic carbon sources such as spatial distribution of litter fall and spatial dependent evapotranspiration rates. This space explicit formulation highlights also the importance of internal fluxes and solute exchange that occur between layers that can trigger instabilities not expected in the single layer formulation.

Finally, by means of the Nernst equation, the time-resolved dynamics of the Fe^{2+}, Fe^{3+} redox reaction allows to predict the rate change of the redox potential when the system is subjected to regular oxic/anoxic oscillations. The output of the model is then compared with a space-time data series of soil moisture and redox potential measured in a column experiment.

Keywords

Soil moisture, dissimilatory iron reduction, hydrologic and redox cycles interactions, redox potential, ecohydrological control, soil modelling

Résumé

Dans le sol, différents cycles biogéologiques s'entrecroisent, interagissent et s'influencent mutuellement. Parmi eux, le cycle de réduction dissimilatrice Fe^{2+}/Fe^{3+} joue un rôle clé dans de nombreux processus biogéochimiques, tels que la bioremédiation et la dégradation de la matière organique se produisant dans le sol. Ce cycle est intimement influencé par les conditions écohydrologiques.
Afin de modéliser la dynamique de la réduction dissimilatrice du fer médiée par la biomasse dans des conditions de saturation fluctuante, il est nécessaire d'utiliser des équations qui couplent à la fois les termes de réaction et de transport.
Dans un premier temps, une étude analytique du modèle proposé par Calabrese et Porporato, qui modélise l'évolution temporelle du couple redox Fe^{2+}/Fe^{3+} dans le sol comme un bioréacteur unique, sera réalisée. Après avoir étudié les points fixes des termes réactifs et effectué une analyse d'instabilité des solutions stationnaires, les dynamiques de Fe^{2+}, de Fe^{3+}, du substrat carboné ainsi que de la population de Fe-réducteurs sera simulée dans le cadre de différents scénarios écohydrologiques.
Le modèle sera ensuite étendu à sa formulation spatiale explicite, en hébergeant les termes de réaction dans un cadre de sol multicouche. D'autres simulations seront également effectuées dans différentes conditions écohydrologiques, permettant d'étudier les différences et les défis du modèle mis en œuvre lorsque ce dernier est couplé à la stochasticité des événements pluvieux. Dans un sol multicouche, des différences substantielles apparaissent entre les couches de surface et les couches plus profondes. Ces différences sont données par des entrées hydrologiques différentes et des sources de carbone plus réalistes, tels que la distribution spatiale de la litière et les taux d'évapotranspiration dépendants de l'espace. Cette formulation explicite dans l'espace met également en évidence l'importance des flux internes et des échanges de solutés qui se produisent entre les couches, et qui peuvent déclencher des instabilités non prévues dans la formulation à une seule couche.
Finalement, au moyen de l'équation de Nernst, la dynamique résolue dans le temps de la réaction d'oxydoréduction Fe^{2+}, Fe^{3+} permet de prédire le changement du taux du potentiel d'oxydoréduction lorsque le système est soumis à des oscillations régulières oxique/anoxique. Le résultat du modèle est ensuite comparé à une série de données spatio-temporelles de l'humidité du sol et du potentiel redox, mesurés dans une expérience en colonne.

Mots-clés

Humidité du sol, réduction dissimilatrice du fer, interactions des cycles hydrologique et redox, potentiel redox, contrôle écohydrologique, modélisation du sol.

Acknowledgments

The first person to whom I owe my thanks is Filippo Miele, who has always been available to help and advise me during these months.

I would also like to thank Professor Andrea Rinaldo for allowing me to carry out my Master's project in the Ecohydrology laboratory.

Similarly, Paolo Benettin has also been crucial and I would like to thank him for planning my Master project and helping me.

I would also like to thank Mitra Asadollahi who provided me with the dataset from the HYDRUS software and Ivan Retti for allowing me to use the results of his master project.

Furthermore, I cannot forget Professor Rizlan Bernier-Latmani, Simiao Wang and Manon Frutschi from whom I learned a lot during the sinergia project meetings (bacterial diversity, biogeochemical cycles, etc.).

Contents

1 Introduction

It is commonly accepted that climate changes of the incoming years will affect - and be affected - by hydrological cycling [1], [2]. How these changes affect soil dynamics such as saturation levels, biogeochemical cycles and the evolution of microbial communities is a crucial point. Indeed, rainfall regime naturally influences the saturation levels of the soil and therefore a change in rainfall generates transition between anaerobic and aerobic conditions. This fluctuations in oxygen availability have a direct impact in the redox potential of the soil [3], [4]. The latter, represents the tendency of the soil to accept or donate electrons to the embedded environment and is considered the major marker, if not a driver, of soil microbial activity [5].

The complex structure of the soil, being a porous medium, allows the co-existence of areas with high levels of saturation even during periods without rain. Similarly, during rainy periods, some soil areas may have relatively low saturation. This makes it difficult to predict whether the soil is in aerobic or anaerobic conditions. The influence between climate and soil is then reciprocal, as soil respiration produces CO_2 and thus influences the carbon cycle, which is closely linked to climate change [6]. Indeed, representing soil respiration one of the leading factors in realising CO_2 in the atmosphere, understanding how quickly the microbial community responds and adapts when subjected to environmental changes is therefore crucial, in order to predict soil response to climate change.

Redox cycles, carbon cycle and other biogeochemical process are closely interconnected in the soil [7]. They are governed by soil parameters and interactions with the hydrological cycle, as well as soil surface processes such as plants uptake and evaporation [8]. Further, the change in pH caused by the switching in the oxidation state of ions influences chemical and surface properties of dissolved material affecting the transport and reaction of colloids and bio-colloids in the soil [9], [10].

One of the most important drivers of the reactions taking place in the soil is soil moisture dynamics as it directly impacts the amount of oxygen in the soil and thus it governs transitions between oxic/anoxic conditions [11]. Soil moisture dynamics is governed by the balance between the external positive inputs such as rainfall and negative outputs such as evaporation, transpiration and leakage [12], [8] and it intimately governs the spatial distribution, the temporal availability and the transport of solute dissolved in the liquid phase.

In this context, particular relevance in the panorama of the geochemically process that naturally takes place in soils, aquatic sediments, and subsurface environments is Dissimilatory Fe(III) reduction which is the process by which microorganisms transfer electrons to external ferric iron [Fe(III)], reducing it to ferrous iron [Fe(II)] [13], [14]. It has an important role in the degradation of organic matter as oxidation of natural and contam-

inant organic compounds being, thus, a useful agent for bioremediation of contaminated sedimentary environments [15], and an important plant nutrient at the level of soil surface [16], [17].

In the soil, iron is generally found in the reduced form Fe^{2+} and in the oxidized form Fe^{3+} [18]. The reduced form Fe^{2+} is a product of mineral wheatering [11], [16] and its redox chemistry is mainly controlled by microorganisms [19].
In saturated conditions, oxygen levels in the soil decrease and facultative microorganisms that decompose organic matter switch from oxygen to alternative electron acceptors. If oxygen is not available as an electron acceptor, more energetically profitable - therefore more quickly consumed - alternatives are represented by NO_3^-, Mn^{4+} and finally, Fe^{3+} compounds [20]. It is clear now that catching the timing over which soil moisture crosses specific value of saturation and for how long these saturation levels are maintained is the key point in describing the Fe^{3+}/Fe^{2+} cycles.

In this context of interactions between the different biogeochemical cycles, and the hydrogeological cycle, this project has the ambition to study and model these interactions under different ecohydrological scenarios.

From one side, to the best of our knowledges, the role of Fe^{3+}/Fe^{2+} reduction cycles for microbial activity has been exhaustively explained and modeled in therm of the Dissimilatory iron reduction process. However, its interplay with soil moisture dynamics has been formulated only at the single bioreactor's level [11]. In this formulation, the spatial and temporal evolution of soil moisture dynamics are lumped in a 'single layer' framework . On the other side, there is a robust past and recent literature on explicit spatial schemes to model soil moisture dynamics [21], [22], [23], that resolves depth's dependency of moisture level and flux exchange between different layers.

Under this perspective, the motivation of this work becomes straightforward and aims to formulate a model that couples spatial distribution of soil moisture, transport process and Fe2-3 dynamics. Before that, we will introduce in the next chapter the spatial lumped model formulated by Calabrese and Porporato [11] focusing on the coupling between hydrological process and reaction terms.

2 The Model for Fe^{2+} - Fe^{3+} reduction

The reference model for the Fe^{2+} - Fe^{3+} cycle studied is the one referred to the "Dissimilatory iron reduction" that has been formulated by Calabrese and Porporato [11] where the time evolution of the concentrations of the two species is encoded in terms of coupled non linear ordinary differential equations (ODES). Although the choice of non linear coupling, rather than simply linear relation, might be arbitrary, it turns out that they better describe more realistic scenarios of concentration's dependent dynamics.

2.1 Iron balance equation

The balance equation for Fe^{2+} iron is modelled as follows:

$$\frac{dFe^{2+}}{dt} = MW + RED - OX - UP - L_{Fe^{2+}} \tag{1}$$

$$\frac{dFe^{3+}}{dt} = OX - RED \tag{2}$$

Iron Fe^{2+} dynamics is characterised by a positive and constant increasing rate coming from the mineral weathering, MW, which represents the release of iron from Fe-minerals present in the soil. Being MW a term that varies very slowly over time compared to the rest of the iron dynamics is considered constant in this model. Furthermore, the redox couple $Fe^{2+} - Fe^{3+}$ must then to include the terms of the reduction (RED) and the oxidation (OX) which describe the rate at which Fe^{3+} is reduced to Fe^{2+} and the latter is oxidised into Fe^{3+} respectively. The two reactions may happen simultaneously and the two terms will appear in the evolution of concentration of both the two species (obviously, with opposite signs). Under the assumptions that reduction is a process biomass mediated while oxidation can happen faster by and it is induced by just oxygen availability, the explicit equation for RED and OX are the following:

$$RED = f(s) \cdot k_{red} \cdot BM \cdot C \cdot Fe^{3+} \tag{3}$$

and

$$OX = g(s) \cdot k_{ox} \cdot (Fe^{2+} - Fe_r^{2+}) \tag{4}$$

.

The reduction rate, RED, is considered to be the multiplication of the amount of substrate carbon C, of Fe-reducers (or biomass) BM, and the amount of Fe^{3+} available. As reducing conditions occurs in high saturation levels, a further term f(s) is multiplied that is a function of the soil moisture. The oxidation rate, OX, is proportional to the difference

between the amount of Fe^{2+} in the soil and a constant amount of Fe_r^{2+} considered resistant to oxidation. Then, as oxidation is triggered at low saturation levels, a modulating function g(s) is multiplied.

The modulating functions $f(s)$ and $g(s)$ depend on soil moisture and describe the presence and influence of oxygen available in the soil for reduction and oxidation, at respectively high and low soil moisture values. The following equations are thus employed:

$$f(s) = \begin{cases} 0 & if\ s < s_{fc} \\ (\frac{s-s_{fc}}{1-s_{fc}})^{\beta} & if\ s \geq s_{fc} \end{cases} \tag{5}$$

$$g(s) = \begin{cases} 1 & if\ s < s_{fc} \\ 1 - (\frac{s-s_{fc}}{1-s_{fc}})^{\zeta} & if\ s \geq s_{fc} \end{cases} \tag{6}$$

Soil field capacity s_{fc} is included in this process as a threshold parameter, which imposes that for low saturation levels reduction does not take place and oxidation is not limited by oxygen.

Finally, as Fe^{2+} is present as released in the liquid phase in its equation there are two negative terms in eq. (1), UP and $L_{Fe^{2+}}$ which represent the iron Fe^{2+} lost from the soil through respectively plant uptake and leakage.

2.1.1 Carbon and Biomass dynamics

The balance equations for organic carbon and the population of Fe-reducers (also biomass) are as follows:

$$\frac{dC}{dt} = ADD + BD - DEC_{aer} - DEC_{red} \tag{7}$$

$$\frac{dBM}{dt} = G_{BM} - BD \tag{8}$$

With regard to carbon dynamics, there are two positive terms, litter fall ADD, which considers the deposition of plants, leaves and residues as a source of organic carbon, and biomass decay BD,

$$BD = k_{BD} \cdot BM \tag{9}$$

which represents the proportion of carbon that becomes available after the death of microbes which is modeled as a first order decay rate with constant rate k_{BD}. Carbon is then consumed by aerobic respiration DEC_{aer},

$$DEC_{aer} = k_{aer} \cdot \phi(s) \cdot C \tag{10}$$

which is proportional to the carbon present in the soil C times decomposition rate k_{aer} and depends on soil moisture according to the modulation function $\phi(s)$,

$$\phi(s) = \begin{cases} \frac{s}{s_{fc}} & if\ s < s_{fc} \\ \frac{1-s}{1-s_{fc}} & if\ s \geq s_{fc} \end{cases} \tag{11}$$

The choice of $\phi(s)$ reflects that aerobic respiration is considered to be linearly increasing in aerobic condition and hyperbolically decreasing for high soil moisture level. The consumption of carbon for the dissimilatory reduction, DEC_{red}, is the proportional to the term RED:

$$DEC_{red} = \alpha \cdot RED \tag{12}$$

time a normalisation factors, α, that represents the grams of carbon decomposed per mole of iron reduced. Finally, the biomass growth is then considered to be proportional to the RED terms as follow :

$$G_{BM} = r \cdot RED. \tag{13}$$

It is important to point out that the choice for the biomass growth of a kinetic equation of a third order, where C, BM and Fe^{3+} are multiplied is not unique. Often, a second order is preferred: in that case the concentration of C (equally for Fe^{3+}), where non limiting the reaction, can be included in the definition of the biomass growth rate. Otherwise, other authors adopt for the Fe^{3+} [24] or carbon concentration [7] a Michaelis–Menten rate equation [25] if concentration of the substratum can represent a limiting factor. In the event that the biomass growth is limited by other finite size effects, a more suitable solution is represented by a logistic equation for BM where the growth asymptotically converges as the biomass reaches his carrying capacity.

2.2 Hydrological equations

For soil moisture, the more general balance equation is as follows:

$$\eta \cdot Z \cdot \frac{ds}{dt} = R - Q - E - T - L \tag{14}$$

where η is the soil porosity, Z the soil depth, R is the rainfall and Q is the runoff, i.e. the part of the rainfall that does not infiltrate the soil. The term leakage/percolation, L, represents the water lost from the soil due to gravity when soil moisture is greater than the soil field capacity. Transpiration, T, is water removed from the soil through plants and the parameter E represents the evaporation. Note that the total volume of water per unit ground area is given by the product $\eta \cdot Z \cdot s$.

As in previous studies [12], [8] all this term will be reduced to exponential (for the leakage) or polynomial expression (for evaporation and transpiration) of the soil moisture. Thus, the water removed from the soil by transpiration depends on soil moisture s.

$$T(s) = \begin{cases} 0 & if\ s \leq s_w \\ (\frac{s - s_w}{s^* - s_w}) \cdot T_{max} & if\ s_w < s < s^* \\ T_{max} & if\ s \geq s^* \end{cases} \tag{15}$$

There are two reference thresholds which are the soil wilting point, s_w, and the point of incipient water stress s^*. If the soil moisture is lower than the soil wilting point the transpiration is zero, if the soil moisture is higher than the point of incipient water stress the transpiration is maximum, T_{max}, and equal to the potential transpiration.

Evaporation is similar but with different threshold values: the soil hygroscopic point, s_{hp}, as the first threshold and the soil wilting point, s_w, as the second threshold, after which evaporation is maximum E_{max}.

$$E(s) = \begin{cases} 0 & if\ s \leq s_{hp} \\ (\frac{s - s_{hp}}{s_w - s_{hp}}) \cdot E_{max} & if\ s_{hp} < s < s_w \\ E_{max} & if\ s \geq s_w \end{cases} \tag{16}$$

Concerning the water loss due to leakage/percolation, this also depends on soil moisture, s, and only starts when soil moisture exceeds the soil field capacity, s_{fc}, which is the threshold after which the soil starts draining by gravity [26].

$$L(s) = \begin{cases} 0 & if\ s < s_{fc} \\ K_{sat} \cdot (\frac{s - s_{fc}}{1 - s_{fc}})^c & if\ s \geq s_{fc} \end{cases} \tag{17}$$

Leakage is proportional to saturated hydraulic conductivity and, as mentioned, increases exponentially, according to the leakage exponent c, with increasing soil moisture.

In some scenarios that will be illustrated in this document, starting from a stochastic rainfall, the above equation will be applied to obtain a soil moisture series. In other cases a soil moisture series already available will be used directly.

2.2.1 Plant Uptake, UP

The plant uptake (UP) represents the amount of iron Fe^{2+} subtracted by plants from the soil as they take up water from the soil via their roots (transpiration). The value is proportional to the concentration of iron Fe^{2+} in the soil and it is modelled as follows:

$$UP = T(s) \cdot [Fe^{2+}] = T(s) \cdot \frac{Fe^{2+}}{\eta \cdot s \cdot Z_r} \tag{18}$$

where T(s) is the transpiration rate computed according to the eq. (15), η the soil porosity, s the soil moisture and Z_r the depth of root zone. The total volume of water per unit ground area is given by the product $\eta \cdot s \cdot Z_r$.

2.2.2 Loss of Fe^{2+} via Percolation/Leakage

Part of the iron Fe^{2+} contained in the soil is lost due to leakage. This loss is proportional to the percolation rate and the to concentration of iron in the soil and it is modelled as

follows:

$$L_{Fe^{2+}} = L(s) \cdot [Fe^{2+}] = L(s) \cdot \frac{Fe^{2+}}{\eta \cdot s \cdot Z} \tag{19}$$

where L(s) is the percolation/leakage rate computed according to the eq. (17), η the soil porosity, s the soil moisture and Z the soil depth. The total volume of water per unit ground area is given by the product $\eta \cdot s \cdot Z$.

3 Methodology

After the model's formulation, its equations will be analytically studied in order to gain a better understanding of its behaviour. First of all, the stationary solutions, i.e. the fixed points, of the system will be derived in order to analytically derive toward which configurations the system will evolve in the absence of external perturbations. In addition, a qualitative instability analysis will be carried out on the restricted carbon-biomass system that dictates whether and when the system will converge or not toward a stable solution. This analytical study will therefore allow us to know in advance what the results of the most simplistic simulations may be, and will also be useful for interpreting simulations of more complex scenarios.

Several different scenarios will be simulated in order to i) validate the results of the analytical calculations and ii) to have reference outputs and to analyse the influence of some key parameters on the model. Particularly:

- to provide insights about the impact of each single process to the overall dynamics.
- to yield a tool to interpret experimental data collected from column to field scale.

By considering soil as a single bioreactor, scenarios with more realistic ADD term with constant soil moisture are modeled as they represent suitable conditions for laboratory scale where both soil moisture and organic carbon supply can be controlled during the soil preparation and the ongoing experiment.

Differently, scenarios characterised by stochastic rainfall regime and seasonal variations for litter fall are included as though to be more appropriate for field experiments.

The model will be then formulated on a 1D vertical lattice support that represents the different layers along the depth. In this case, evapotranspiration will be included in the top two layers and the role of internal fluxes and the differences in inputs for the different layers will be studied.

Finally, the model will be fed with a previously collected dataset of soil moisture oscillations where oxic/anoxic phases cyclically alternated in a lysimeter experiment. The simulated time evolution of the concentrations of the two species Fe^{2+}-Fe^{3+} will be used to extrapolate information on the rate of change of redox potential and the results will be compared with the time series of fluctuating redox potential that has been monitored during the same experiment.

4 Fixed point characterization

4.1 Fixed point derivation

The nonlinearities of the systems of equations (1), (2), (7) and (8) can be a priori handled by an instability analysis to understand whether and when the system converges to a steady state solution [27]. To better understand at which level transport and reaction are interconnected, the analysis for the reaction term only is firstly developed and later including the transport terms. The steady state solution is the condition where all the time derivatives (eq. (1), (2), (7) and (8)) are equal to zero. It's clear that, by neglecting the UP and L terms in eq. (1) there is not fixed point solution for the couple Fe^{2+}/Fe^{3+} as Fe^{2+} reaches the equilibrium if $RED - OX$ compensate the MW term leading a divergency in the Fe^{3+} for t to infinity. On the same line as the analysis performed by Manzoni et. al. in [7] where a similar model has been adopted for the carbon-nitrogen cycle in microbe-plant competition, a constant Fe^{3+} concentration is then assumed, since Fe^{3+} is the fundamental electron acceptor that triggers the Fe^{2+}/Fe^{3+} cycle. Under this asumption the steady state solutions for the C, BM and Fe^{2+} term are the following:

$$C = \frac{a_0}{Fe^{3+}} \tag{20}$$

where $a_0 = \frac{k_{BD}}{r \cdot f(s) \cdot k_{red}}$,

$$BM = a_1 + \frac{a_2}{Fe^{3+}} \tag{21}$$

with $a_1 = \frac{-ADD}{k_{BD} - \frac{\alpha \cdot k_{BD}}{r}}$ and $a_2 = \frac{k_{aer} \cdot \phi(s) \cdot k_{BD}}{r \cdot f(s) \cdot k_{red} \cdot (k_{BD} - \frac{\alpha \cdot k_{BD}}{r})}$ respectively, and

$$Fe^{2+} = a_3 + \frac{a_4}{Fe^{3+}} \tag{22}$$

where $a_3 = \frac{MW + \frac{k_{BD}}{r} \cdot a_1}{g(s) \cdot k_{ox}} + Fe_0^{2+}$ and $a_4 = \frac{\frac{k_{BD}}{r} \cdot a_2}{g(s) \cdot k_{ox}}$.

Finally, including the $L_{Fe^{2+}}$ term, it is possible to derive the following steady solution for Fe^{2+}:

$$Fe^{2+} = a_5 + \frac{a_6}{Fe^{3+}} \tag{23}$$

where $a_5 = \frac{MW + \frac{k_{BD}}{r} \cdot a_1 + Fe_r^{2+} \cdot g(s) \cdot k_{ox}}{g(s) \cdot k_{ox} + \frac{L(s)}{\eta \cdot s \cdot Z_r}}$ and $a_6 = \frac{\frac{k_{BD}}{r} \cdot a_2}{g(s) \cdot k_{ox} + \frac{L(s)}{\eta \cdot s \cdot Z_r}}$.

In this case, when MW is equal to $L_{Fe^{2+}}$ combining eq. (1) and (2), it is possible to zero out the derivative of Fe^{3+} thus making the Fe^{3+} concentration converge. Indeed,

$$MW - L_{Fe^{2+}} = OX - RED \tag{24}$$

and thus, if $MW = L_{Fe^2+}$, it turns out that:

$$\frac{dFe^{3+}}{dt} = OX - RED = 0$$

It's straightforward to extend the result including the UP contribution by replacing L with the sum of all negative terms that comes from the transport process.

As expected and previously proved by Manzoni and D'Odorico in [7], [28], all the constants appearing in solutions are functions of the time dependent variables ADD and s.

By numerically implementing the model of eq. (1), (2), (7), (8) with a time Euler forward scheme written in MATLAB, it is possible to verify the results (see figure 2). Table 1 lists the values used within the framework of this project, any specific changes for certain scenarios will be reported within the specific chapter. The parameters are mainly taken from the reference in [11], the normalization factor (w) for the BM to convert number of cells into kg of carbon when this appears in the term RED has been roughly estimated. To verify the consistency of our implementation, in figure 1 is shown the result of our calibration with s=1 to fit the data from the work of Ginn et. al. [29]. The plot in figure 1 shows the same agreement as the one showed in the work of Calabrese and Porporato [11].

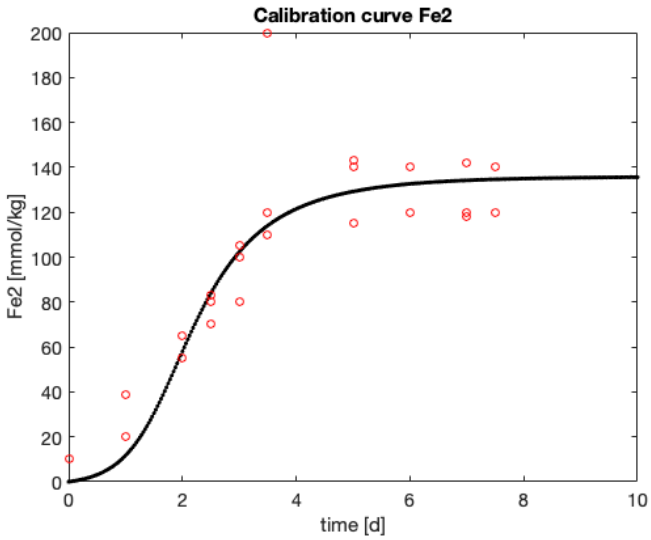

Figure 1: Calibration curve: the model is calibrated to reproduc the dataset of [29].

In figure 2, instead, one can observe the dynamics of the variables for the two cases mentioned, without $L_{Fe^{2+}}$ and with $L_{Fe^{2+}}$ = MW, in a scenario with constant soil moisture s=0.9, and constant litter fall.

Parameter	**Symbol**	**Value**	**Units**
Porosity	η	0.48	-
Soil field capacity	s_{fc}	0.8	-
Soil hygroscopic point	s_{hp}	0.36	-
Soil wilting point	s_w	0.42	-
Point of incipient water stress	s^*	0.76	-
Saturated hydraulic conductivity	K_{sat}	0.045	m/d
Leakage exponent	c	6	-
Amount of Fe^{2+} resistant to oxidation	Fe_r^{2+}	0.05	mmol/kg
Biomass decay rate	k_{bd}	0.023	1/d
Parameter for reduction limitation f(s)	β	2	-
Parameter for oxidation limitation g(s)	ζ	4	-
Aerobic decomposition rate	k_{aer}	$2.7 \cdot 10^{-4}$	1/d
Carbon decomposition rate	α	0.1	1/d
Growth Fe reducers rate	r	$4 \cdot 10^{10}$	cell/mmoles
Mineral weathering	MW	0.08	mmol/kg/d
Reduction rate constant	k_{red}	$8.89 \cdot 10^{-15}$	$kg^2/cells/g/d$
Reduction rate after normalizing BM	$k_{red,norm}$	0.2	$kg^2/cells/g/d$
Oxidation rate constant	k_{ox}	$4.32 \cdot 10^1$	1/d

Table 1: Parameters used to make the simulations, any changes will be specified in the chapter of interest.

First of all Fe^{3+} meets the expectations, in the case without $L_{Fe^{2+}}$it diverges with a slope proportional to the MW, while in the case with $L_{Fe^{2+}}$ = MW the derivative of Fe^{3+} can be equal to 0 at the same time as the derivative of Fe^{2+} is equal to 0, so Fe^{3+} converges. C fixed point is inversely proportional to Fe^{3+}, once the system has reached "equilibrium", in the case without $L_{Fe^{2+}}$ given the increasing trend of Fe^{3+}, carbon has a decreasing trend. The relationship found analytically is also confirmed in the case with $L_{Fe^{2+}}$ = MW. It can be seen that for a converging Fe^{3+}, C also converges.

At equilibrium the biomass is equal to the sum of a constant (a_1) and another constant (a_2) divided by Fe^{3+}. This means that if the concentration of Fe^{3+} is large enough as in the case of the scenario without $L_{Fe^{2+}}$ in figure 2, in which Fe^{3+} has an increasing trend, the biomass can be approximated to the constant a_1. Even in the case of a convergence of Fe^{3+}, the biomass tends to a constant. The two constants to which it tends in the two cases, are similar but not the same, this is due to the fact that Fe^{3+} has a small influence. Since the derivative of Fe^{2+} depends directly on $L_{Fe^{2+}}$, the solutions at equilibrium are different in cases where the leakage term is present or absent. However, both are in the same form, a constant a_3 (and a_5) plus another constant a_4 (and a_6) divided by Fe^{3+}. Fe^{2+} is expected to converge to a value close to the constant a_3 (or a_5) when the concentration of Fe^{3+} is sufficiently high as in the cases of the scenarios simulated in figure 2.
Finally, it can be observed that for the parameters used Fe^{2+}, C and BM oscillate before falling on their fixed point. In the next section, this phenomenon, among others, will be investigated.

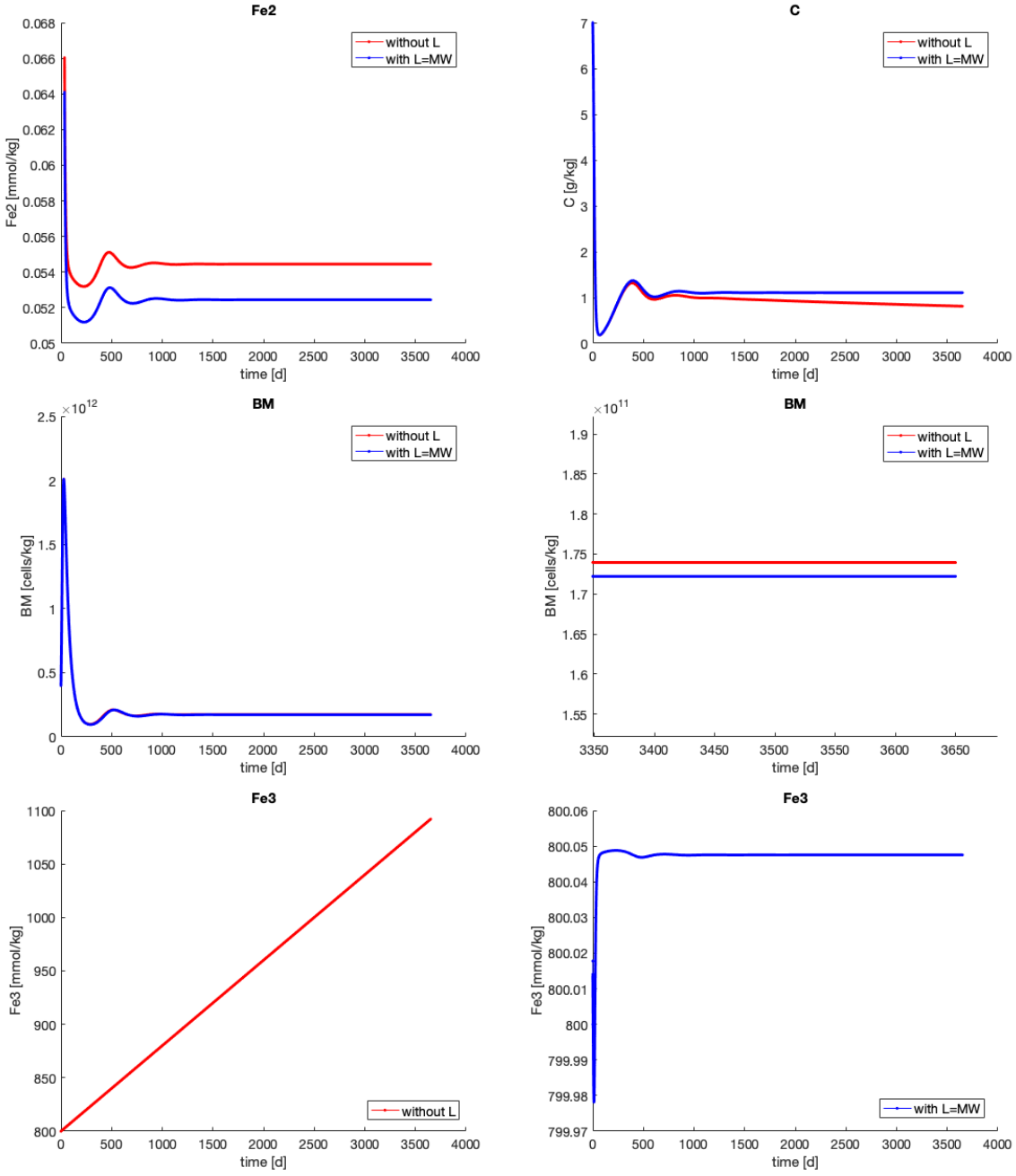

Figure 2: Fixed point validation with a constant soil moisture s=0.9. The red colour represents a scenario without $L_{Fe^{2+}}$, while the blue colour represents a scenario with $L_{Fe^{2+}} = MW$. Top left: time evolution of Fe^{2+} - Top right: time evolution of C - Center left: time evolution of BM - Center right: zoomed time evolution of BM - Bottom left: time evolution of Fe^{3+} (without $L_{Fe^{2+}}$) - Bottom right: time evolution of Fe^{3+} ($L_{Fe^{2+}} = MW$).

4.2 Instability analysis

Taking a cue from the instability analysis done by Manzoni and Porporato [7], it is possible to analyse the Carbon and Biomass couple of equations under the assumption of a constant Fe^{3+} concentration. For this purpose, we will perform an instability analysis to predict whether and how the equilibrium is reached. This can be achieved by a standard perturbation approach where the dynamics of the nonlinear term is linearized near the steady state solution. To avoid a heavy notation, the step behind this technique can be briefly summarised by referring to the following generic reaction equations:

$$\begin{cases} \dfrac{\partial C(t)}{\partial t} = u\left(C(t), BM(t)\right) \\ \\ \dfrac{\partial BM(t)}{\partial t} = u\left(C(t), BM(t)\right) \end{cases} \tag{25}$$

By Taylor expansion the reaction terms, the early evolution of a perturbation defined as $\delta C = C - C^*$ and $\delta BM = BM - BM^*$ is governed by the following equation

$$\begin{pmatrix} \dot{\delta C} \\ \dot{\delta BM} \end{pmatrix} = \boldsymbol{J} \begin{pmatrix} \delta C \\ \delta BM \end{pmatrix} \tag{26}$$

where the dot represent the time derivative and $\boldsymbol{J}$ is the usual Jacobian matrix defined as:

$$\boldsymbol{J} = \begin{pmatrix} u_C & u_{BM} \\ v_C & v_{BM} \end{pmatrix}.$$

evaluated in (C^*, BM^*). The system (26) admits solution that can be expressed in terms of exponential function:

$$\begin{pmatrix} Ae^{-\lambda_1 t} \\ Be^{-\lambda_2 t} \end{pmatrix}$$

and their time evolution is governed by the *Real* and *Imaginary* part of the eigenvalues λ_1 and λ_2. If the real part of the eigenvalue is negative the system is stable, if the real part is positive the system is unstable. Furthermore, if the imaginary part is non-zero, the system achieves stability by means of an oscillation, otherwise with an exponential convergence.

By considering then the model of Calabrese and Porporato composed of eq. (7) and (8):

$$\begin{cases} \frac{dC}{dt} &= ADD + BD - DEC_{aer} - DEC_{red} \\ \frac{dBM}{dt} &= G_{BM} - BD \end{cases}$$

and combining the eq. (10), (12), (9), (13), the Jacobian reads as follows:

$$J = \begin{bmatrix} -k_{aer} \cdot \phi(s) - \alpha \cdot f(s) \cdot k_{red} \cdot BM \cdot Fe^{3+} & k_{BD} - \alpha \cdot f(s) \cdot k_{red} \cdot C \cdot Fe^{3+} \\ r \cdot f(s) \cdot k_{red} \cdot BM \cdot Fe^{3+} & r \cdot f(s) \cdot k_{red} \cdot C \cdot Fe^{3+} - k_{BD} \end{bmatrix} \tag{27}$$

with the eigenvalues:

$$\lambda_{1,2} = \left[\frac{\omega + \frac{\alpha\cdot(\frac{\omega}{r}-\mu)}{1-\frac{\alpha}{r}}}{2\cdot k_{bd}}\right] \pm \left[\left(\frac{\omega + \frac{\alpha\cdot(\frac{\omega}{r}-\mu)}{1-\frac{\alpha}{r}}}{2\cdot k_{bd}}\right)^2 + (\omega - r\cdot\mu)\right]^{1/2} \tag{28}$$

where:

$$\omega = k_{aer}\cdot\phi(s)\cdot k_{bd} \tag{29}$$

and

$$\mu = ADD\cdot f(s)\cdot k_{red}\cdot Fe^{3+} \tag{30}$$

The condition for which the imaginary part is non-zero is given by the following inequality:

$$\Delta(s) = \left(\frac{\omega + \frac{\alpha\cdot(\frac{\omega}{r}-\mu)}{1-\frac{\alpha}{r}}}{2\cdot k_{bd}}\right)^2 + (\omega - r\cdot\mu) < 0 \tag{31}$$

It is interesting to note that the soil moisture, which appears implicitly via the functions $f(s)$ and $\phi(s)$, may be responsible for the existence of an imaginary part of the eigenvalues. For a given range of fixed values of s, the variables C and BM will converge oscillating around the fixed point while for other values of s, the convergence will be exponential towards the fixed point. ADD also plays a key role as can be seen in figure 3 which illustrates the dependence of the imaginary part of the eigenvalue on s and ADD.

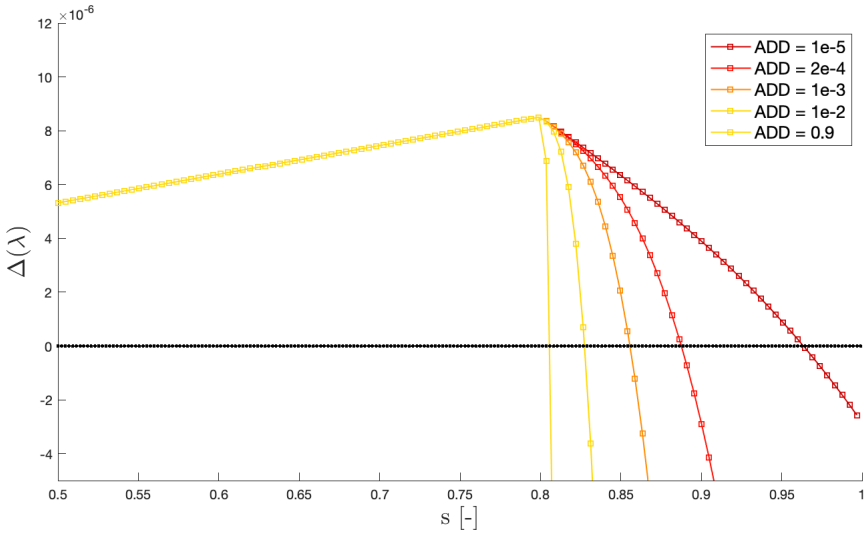

Figure 3: Instability region, Δ, as a function of s for different ADD obtained by numerical integration of eq. (31)*. In the region of the parameters where Δ is above zero, the $Im(\lambda)$ are different from zero and the system converges in an oscillating manner.*

The importance of this analysis resides on the fact that, although oscillation of organic carbon and microbial community are generally associated to changes in external output,

this is not the case. Indeed, the system can exhibits inner fluctuations even for constant environmental conditions, that are triggered by the nested nonlinear behavior of the two species.
Figure 5 illustrates the "C vs BM curve" for a scenario with constant soil moisture and constant ADD. In the figure it can be seen that the type of convergence depends on the value of s. For some soil moisture the convergence is oscillating, for others it is not.

It is worthwhile to mention that by numerical implementation of (3) the real Real part of the eigenvalues is always negative with the following consequence that self sustained oscillations do not persist over time. This is absolutely not surprising as the the system of eq. (7) and (8) resembles a "quasi" Lotka-Volterra type of dynamics where, rather, oscillations persist and are not dumped.
The original formulation of the Lotka-Volterra [25] model must to include in this case a positive term for the carbon, C, which is absent in the present formulation but it comes out when the model will be formulated in the next sessions in its explicit spatial version as an effect of internal fluxes.

To validate the instability analysis, soils with constant soil moisture ranging in the interval between 0.8 and 1 at depth of 0.75 m are chosen.

Scenario with constant soil moisture and constant ADD

The results of the scenario with constant soil moisture and constant ADD are shown in figures 4 and 5. The iron Fe^{3+} increases along the simulation, according to the equation 2, the oxidation term is larger than the reduction term so the concentration increases. The growth rate is similar to the mineral weathering (MW) value, this comes from the equation 1, in fact in this scenario the iron Fe^{2+} converges, its derivative becomes 0, since the value of plant uptake is equal to 0, the Fe^{3+} growth is very close to the mineral weathering value $MW = 0.08$ mmol/kg/d.

$$\frac{dFe^{3+}}{dt} = OX - RED \simeq MW$$

There are smears, not visible, in the Fe^{3+} growth when RED is greater than OX but the general trend of Fe^{3+} corresponds to that of the "$MW \cdot t$" curve.
Iron Fe^{2+} concentration, for soil moisture values of 0.8 and 0.82 falls directly on lower values (first type of convergence), while for the other values of s it can be observed that the concentration tends to stabilise after a period of oscillations (second type of convergence). It can be observed that the duration of the oscillations depends on the soil moisture, the higher the soil moisture the shorter the time the curve takes to stabilise. The constant towards which iron Fe^{2+} tends can be calculated according to the equation 23.
The behaviour of carbon for different soil moisture is conceptually similar to that of Fe^{2+}, in fact for values of s=0.80 and s=0.82 it is observed to be completely different than for the other values of s. Again for soil moisture between 0.84 and 0.90 oscillations occur before an equilibrium is reached and again the higher the soil moisture the shorter the duration of the oscillations. It can be seen from figure 4 that the C trend is slightly negative, this is due to the relation 20, in fact the carbon fixed point decreases when Fe^{3+} increases. The same trend was already observed in the figure 2.

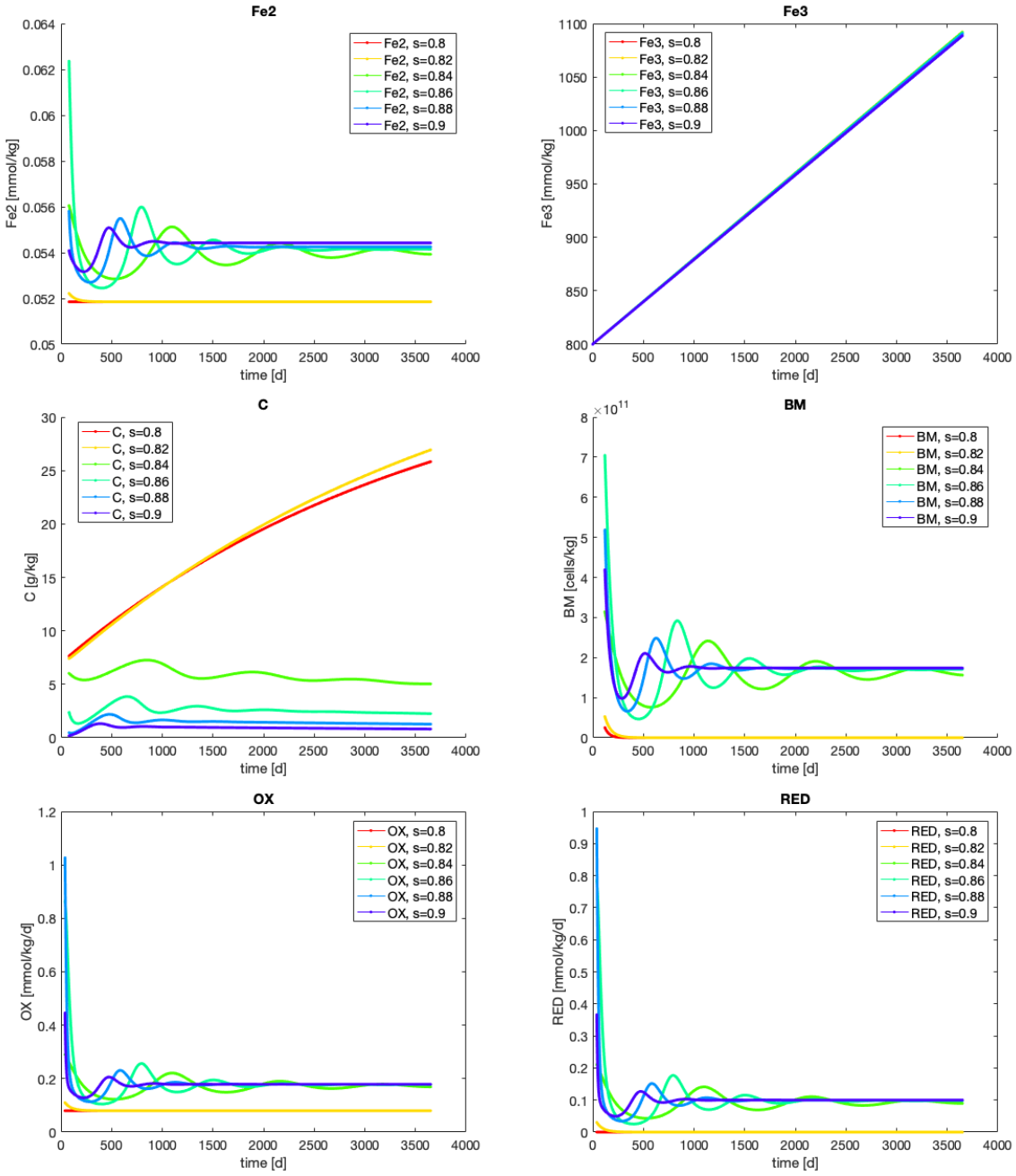

Figure 4: Scenario with constant $ADD = 0.01$ [g/kg/d] , constant s, presence of $L_{Fe^{2+}}$, for a soil depth of 0.75 m. Colorbar represents the pattern for constant but different soil moisture $\in [0.8 - 0.9]$. Top left: time evolution of Fe^{2+} - Top right: time evolution of Fe^{3+} - Center left: time evolution of C - Center right: time evolution of BM- Bottom left: time evolution of OX - Bottom right: time evolution of RED.

Fe^{2+} behaves similarly to BM, this is not surprising as the biomass represents the amount of Fe-reducers, the larger this amount the more iron is reduced to its Fe^{2+} form. Concerning the relationship between C and BM, soil moisture has a direct impact on the eigenvalues of the Jacobian (equation 28) of the carbon-biomass system so it can change the stability of the system and the way the "C vs BM curve" converges towards the fixed points. In figure 5 it can be observed that for some values of s the convergence towards

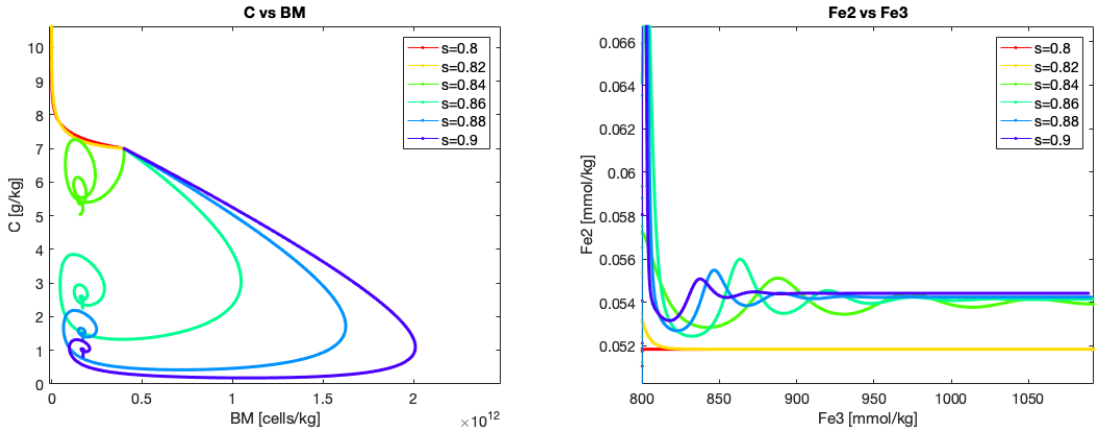

Figure 5: Scenario with constant $ADD = 0.01[g/kg/d]$ *, constant s, presence of* $L_{Fe^{2+}}$*, for a soil depth of 0.75 m. Colorbar represents the pattern for constant but different soil moisture* $\in [0.8 - 0.9]$*. Left: time evolution of C vs BM curve - Right: time evolution of* Fe^{2+} *vs* Fe^{3+} *curve. (All scenarios have the same initial conditions).*

the fixed points occurs through oscillations while for other values of the system it converges exponentially. Note that the simulation is not long enough to see the convergence of some curves.

5 Soil as a single reactor

At the level of soil as a single bioreactor, the scenarios are chosen in order to have an overview of the influence of soil moisture and litter fall on the model, in the light of the results of the fixed points and instability analysis sections. The litter fall is a significant parameter as it is an input that does not depend on soil characteristics and, differently from the kinetic rate that are considered constant, litter fall depends drastically on seasonally time scale in field experiments or in the soil preparation process at column scale experiments. Firstly, different scenarios for the ADD will be explored for constant value of soil moisture. To better observe the effect of soil moisture and litter fall, transpiration and plant uptake is not taken into account in this section. In the second part, fluctuation of soil moisture when soil is subjected to a stochastic rainfall regime will be included and the extent to which the systems are sensitive to the two different external oscillating inputs will be observed.

Litterfall (as ADD source) regimes
In order to study the influence of litter fall (ADD) on the model, two different realistic regimes are explored. The first is characterized by an ADD that decays exponentially over time: this regime is a crude representation of what can be a laboratory experiment on a soil column, with the introduction of an initial amount of ADD that will then be consumed along the experiment. A second regime was chosen with monthly changes: this case is closer to a more realistic seasonal/monthly dynamic, the values are similar to the range of values proposed by Calabrese and Porporato [11] and repeated for 10 years. The two regimes characterized by variations are illustrated in figure 6.

5.1 Scenario with constant soil moisture and ADD that varies monthly

This scenario is characterised by a constant soil moisture and a monthly varying litter fall according to the trend observed in in the right-hand side of the figure 6. Figure 7 shows a larger soil moisture range, in this case from 0.5 to 1, while figures 8 and 10 go into detail about what happens between soil moisture 0.8 and 0.9.
In figure 7, the behaviour of the model can be observed for a soil moisture equal to 1. In that case the oxidation term (equation 4) is equal to 0 because the function g(s) (equation 6) is equal to zero. This represents a completely saturated soil, where oxygen is present in very small quantities, not sufficient to allow the oxidation of iron. It can be seen that Fe^{3+} decreases for a soil moisture = 1 as its derivative becomes equal to:

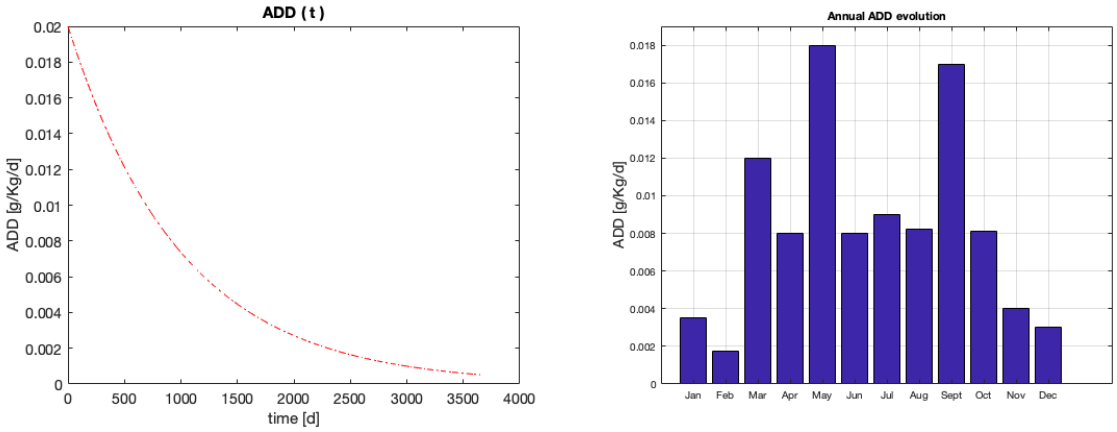

Figure 6: ADD regimes. Left: ADD that decays along the simulation - Right: ADD that varies monthly.

$$\frac{dFe^{3+}}{dt} = OX - RED = -RED$$

There are non-visible smears in the Fe^{3+} growth when RED is greater than OX but the general trend of Fe^{3+} corresponds to that of the "$MW \cdot t$" curve when soil moisture is smaller than 1. This is why the Fe^{3+} plots will not be presented in future simulations as they are repetitive.

In this scenario it can also be seen that the behaviour of the other variables is completely different from soil moisture below 1 compared to when there is a soil moisture equal to 1. In figure 7, not all the curves can be distinguished because they are superimposed. For Fe^{2+} and Fe^{3+} two different behaviours are observed when soil moisture equals 1 or relax to values slightly below 1 (the curve of s=0.9 covers all the others). In the case of the biomass, OX rate and RED rate, the curve of s=0.8 covers all the curves with a lower soil moisture. These considerations are at the origin of the investigation of what happens between a soil moisture of 0.8 and a soil moisture of 0.9. Moreover, it can be observed always in figure 7 the sensitivity of the model to values of s: a change of $\Delta s = 0.1$ can be responsible for completely different responses.

Focusing on the range of soil moisture between 0.8 and 0.9, one can observe the differences between a scenario with constant litter fall (commented above) illustrated in the figure 4 and a scenario with monthly variable litter fall illustrated in the figure 8. It can be seen that litter fall plays an important role in the dynamics of the model variables. In fact, this was already known during the study of fixed points and during the stability analysis, as the relationships found also depended on the litter fall. It is interesting to note that the monthly litter fall evolution observed in the right-hand side of the figure 6 has a clearly visible impact in the carbon, C, curves as shown in figure 8.

Concerning Fe^{2+} and BM, fluctuations of ADD heavily affects their time evolution by governing the curve's course. This is not surprising as the fixed points of Fe^{2+} and BM (equations 23 and 21) depend directly on the value of the ADD. Figure 9 illustrates the effect of ADD on the temporal evolution of the BM for a soil moisture of s=0.9, it can be seen that the BM responds to ADD peaks with a temporal lag.

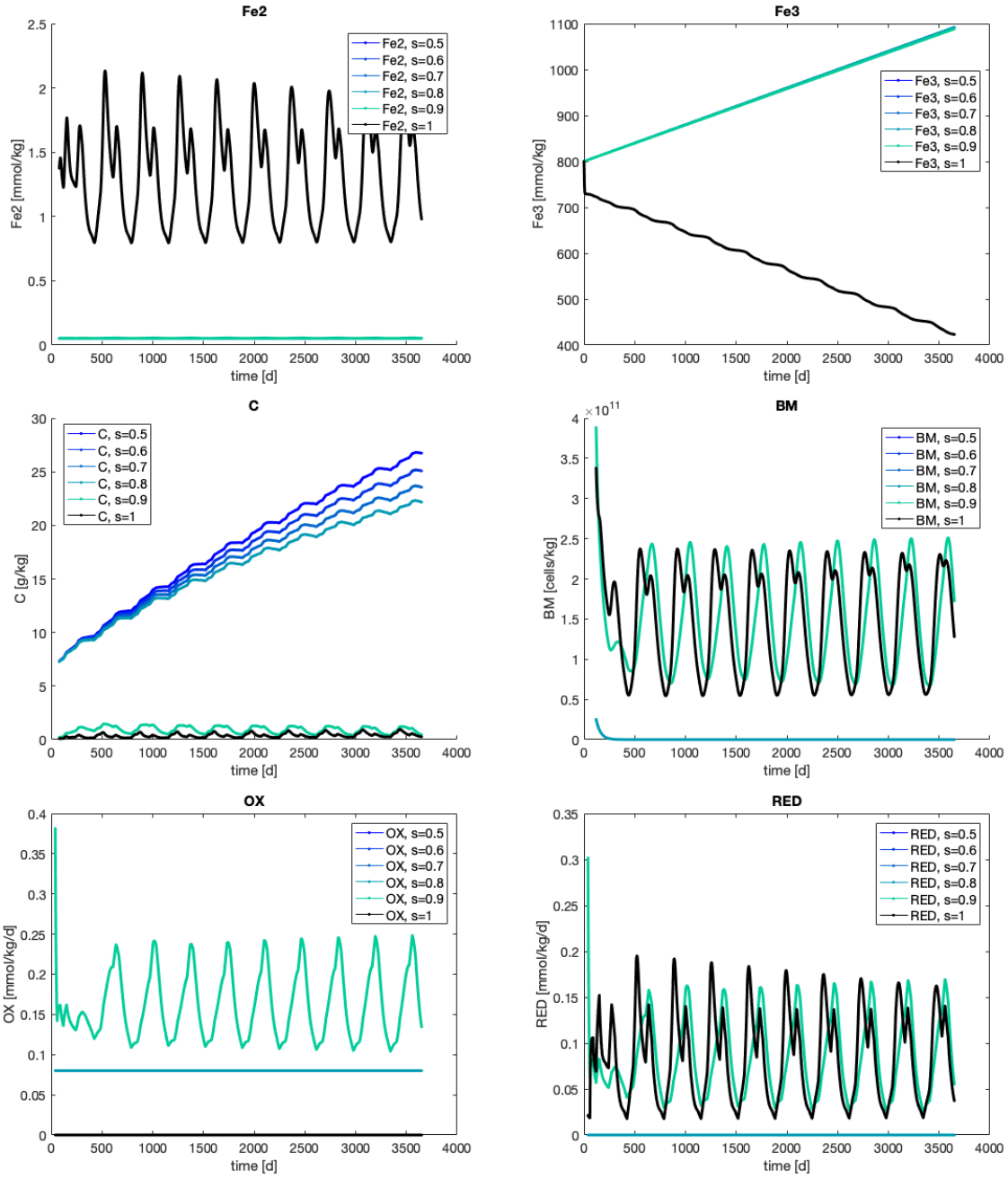

Figure 7: Scenario with ADD that varies monthly, constant s, presence of $L_{Fe^{2+}}$, for a soil depth of 0.75 m. Colorbar represents the pattern for constant but different soil moisture $\in [0.5 - 1.0]$. Top left: time evolution of Fe^{2+} - Top right: time evolution of Fe^{3+} - Center left: time evolution of C - Center right: time evolution of BM- Bottom left: time evolution of OX - Bottom right: time evolution of RED.

With regard to the stability of the carbon-biomass system, one can observe in the figure 10 the "noise" that brings the ADD to oscillatory convergence for soil moisture above 0.84. This is due to the presence of the ADD term in the imaginary part of the eigenvalues (see equations 28 and 31) as expected from the instability analysis.

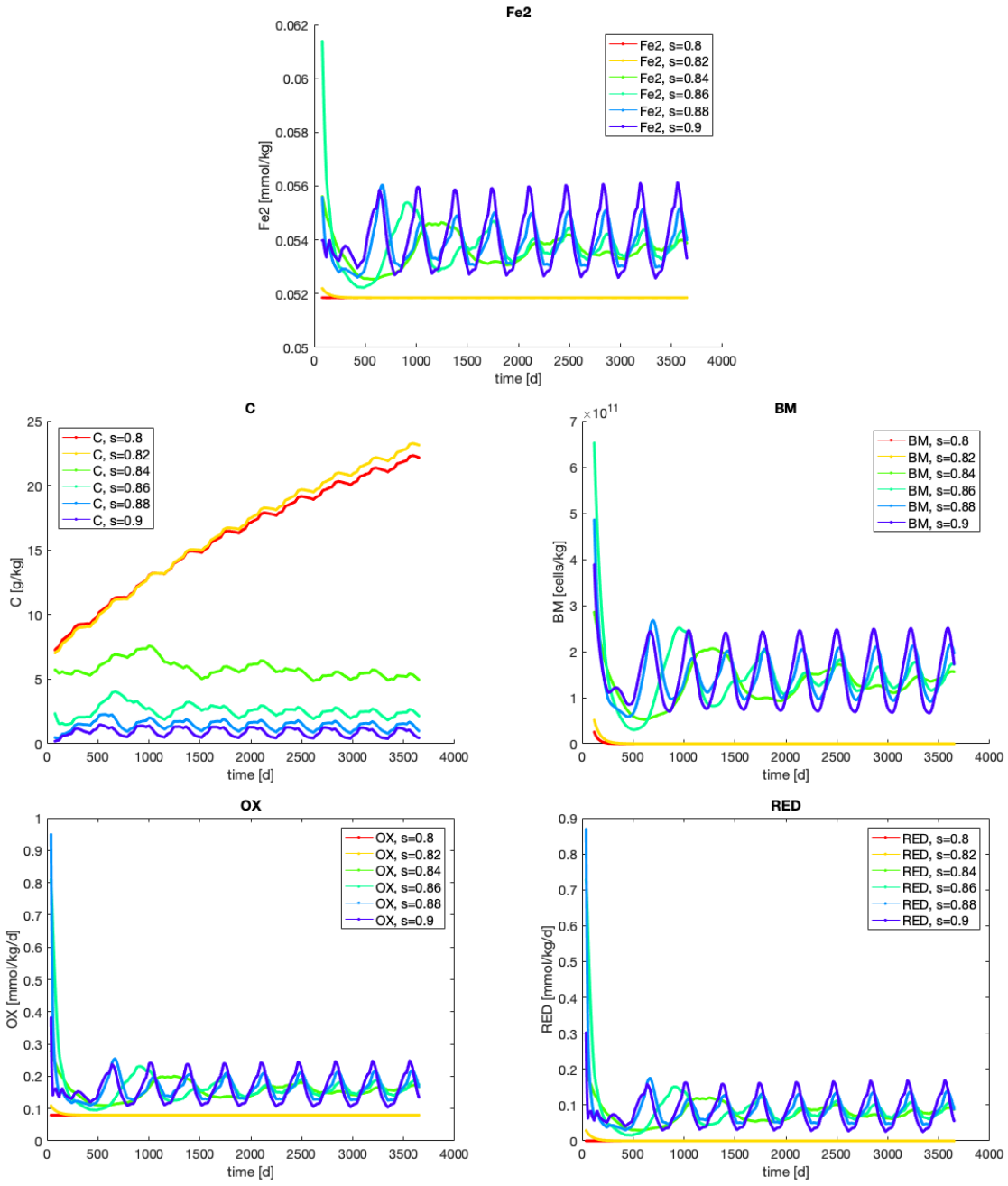

Figure 8: Scenario with ADD that varies monthly, constant s, presence of $L_{Fe^{2+}}$, for a soil depth of 0.75 m. Colorbar represents the pattern for constant but different soil moisture $\in [0.8 - 0.9]$. Top: time evolution of Fe^{2+} - Center left: time evolution of C - Center right: time evolution of BM- Bottom left: time evolution of OX - Bottom right: time evolution of RED.

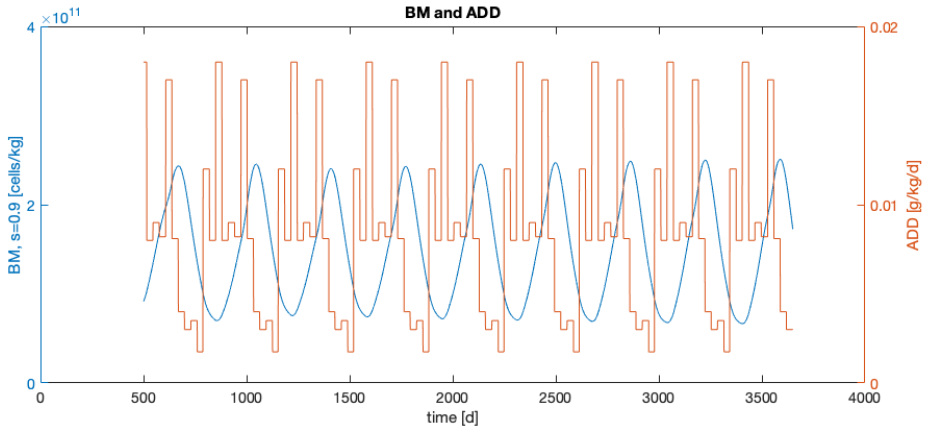

Figure 9: Scenario with ADD that varies monthly, constant s=0.9, presence of $L_{Fe^{2+}}$, for a soil depth of 0.75 m. Effect of ADD on BM.

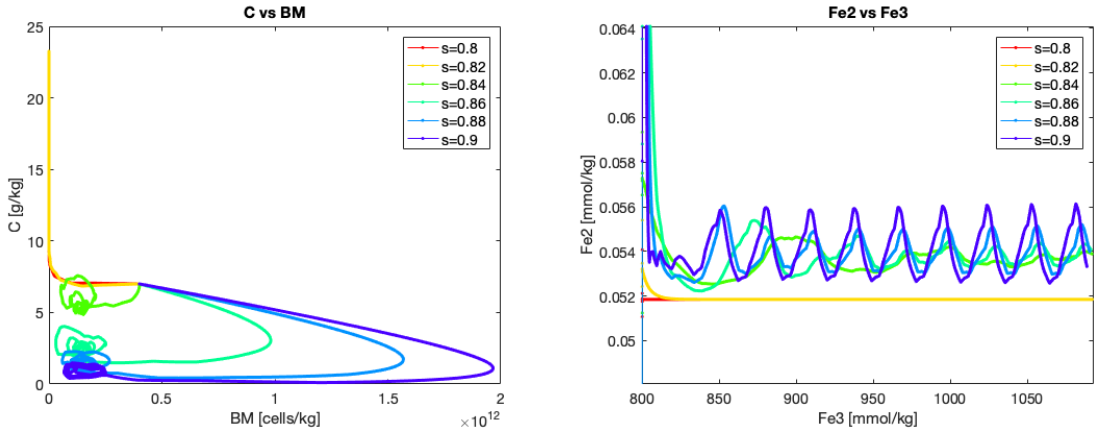

Figure 10: Scenario with ADD that varies monthly, constant s, presence of $L_{Fe^{2+}}$, for a soil depth of 0.75 m. Colorbar represents the pattern for constant but different soil moisture $\in [0.8 - 0.9]$. Left: time evolution of C vs BM curve - Right time evolution of Fe^{2+} vs Fe^{3+} curve.

5.2 Scenario with constant soil moisture and ADD that decays

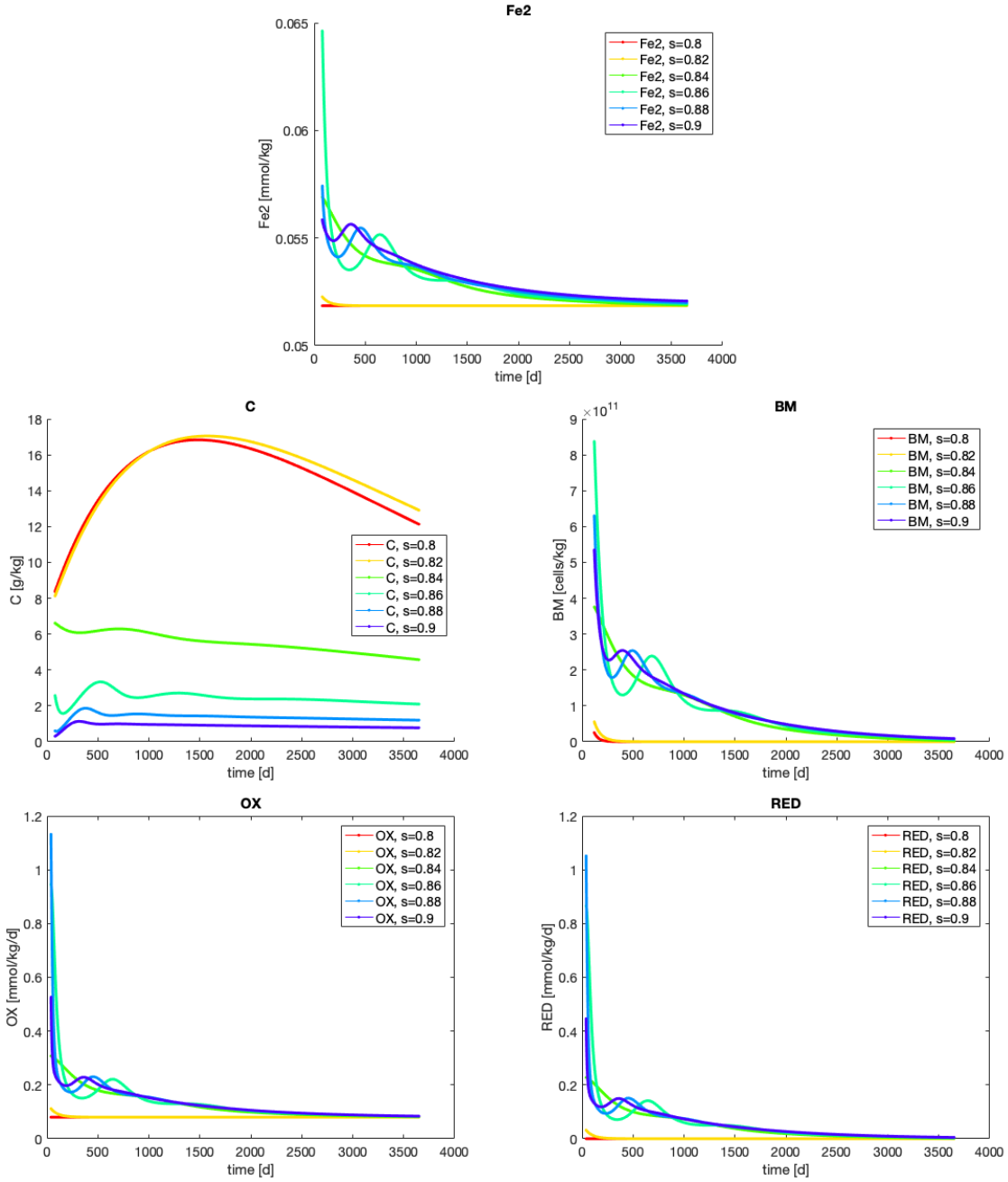

Figure 11: Scenario with ADD that decays, constant s, presence of $L_{Fe^{2+}}$, for a soil depth of 0.75 m. Colorbar represents the pattern for constant but different soil moisture $\in [0.8 - 0.9]$. Top: time evolution of Fe^{2+} - Center left: time evolution of C - Center right: time evolution of BM - Bottom left: time evolution of OX - Bottom right: time evolution of RED.

This scenario is characterised by a constant soil moisture and a litter fall that decays according to the trend observed in the left-hand side of the figure 6. Figures 11 and 12 refer to this scenario. In the figure 11 the trends are very similar to the scenario with constant ADD, but one can see the form of decay given by the ADD in the plots of Fe^{2+} and BM. Very interesting is what occurs in the figure 12: for soil moisture above 0.84 the carbon-biomass system starts to converge with oscillations that vanish when the ADD falls below a certain threshold and starts to converge exponentially. Of course, the point

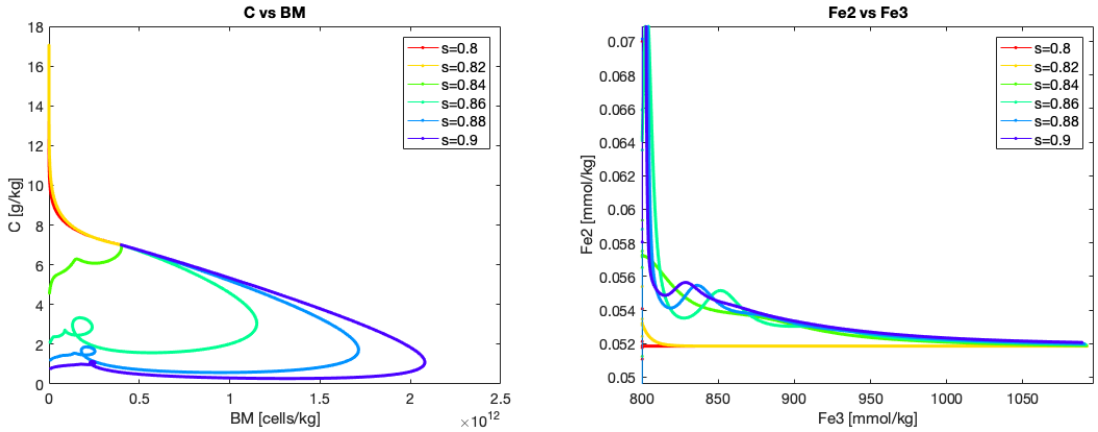

Figure 12: Scenario with ADD that decays, constant s, presence of $L_{Fe^{2+}}$, for a soil depth of 0.75 m. Colorbar represents the pattern for constant but different soil moisture $\in [0.8 - 0.9]$. Left: time evolution of C vs BM curve - Right: time evolution of Fe^{2+} vs Fe^{3+} curve.

of convergence also depends on the ADD and varies throughout the simulation. The threshold of the ADD, responsible for the different behaviours, can be estimated from the equation 31 or from figure 3.

5.3 Scenario with variable soil moisture (stochastic rainfall)

A scenario with variable soil moisture induced by a stochastic rainfall series following a Poisson distribution is finally simulated. This Poisson process is characterized by the frequency λ, representing the inverse of the mean inter-arrival times between two subsequent rainfall events, and random rainfall intensity that are exponentially distributed with the constraint that the total amount of water precipitated P_{year} is fixed. The parameters of the rain are listed in the table 2. The annual rainfall is set at 1.1 m/y, and is based on a value that can be compared to annual rainfall in Switzerland. The average interval between events is set at 5 days.

Parameter	Symbol	Value	Units
Mean annual precipitation	P_{year}	1.1	m/y
Mean interval between events	interarr	5	d
Number of downscalings of daily precip.	n_{down}	5	-

Table 2: Parameters used to make the stochastic rainfall

Unlike the previous scenarios a more realistic scenario is approached, with variations of soil moisture due to stochastic rainfall data set. The simulation is done for a 0.75 m deep soil and with a litter fall that varies monthly (see right-hand side of figure 6) and without considering evapotranspiration. For this scenario the leakage exponent is set at $c = 3$, which is different from the previous scenarios (see table 1).

First of all, it is necessary to comment on the soil moisture series, illustrated in figure 13, for which it can be observed that the soil moisture varies between values of approximately 0.83 and 1. For most of the time, with the exception of a few moments at the beginning resulting from the initial conditions, the soil moisture is above the value of the soil field

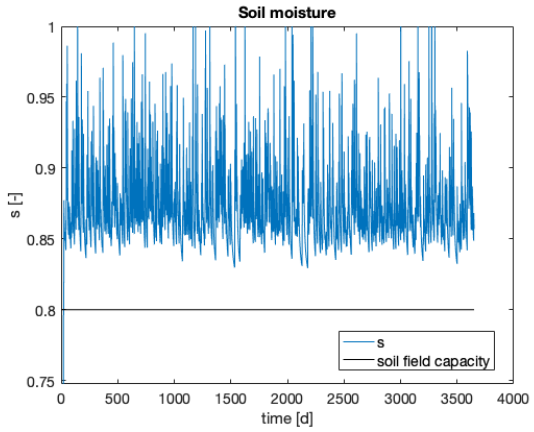

Figure 13: Scenario with s calculated from a stochastic rainfall, with ADD that varies monthly, presence of $L_{Fe^{2+}}$, soil depth= 0.75 m, without evapotranspiration. Blue line is the time evolution of soil moisture, black line is the soil field capacity.

capacity. A first consequence is that the functions g(s) (eq. (6)) and f(s) (eq. (5)) do not take on constant values respectively of 1 and 0 this is because $s > s_{fc}$. At peaks of soil moisture, when it equals 1, oxidation OX is zero and reduction RED will be at full capacity. Furthermore, covering the range between 0.83 and 1 and considering the differences found in the previous scenarios for this soil moisture range different model responses will alternate during the simulation.

In the Fe^{2+} dynamic it can be observed that several peaks occur along the simulations, however Fe^{2+} fails to accumulate, and immediately after the peaks it falls. Oxidation prevails over reduction, even though the soil moisture range is high. In fact, the times when oxidation is greater than reduction are sufficient to consume almost all the Fe^{2+}, which may then rise again with another peak but will also be consumed. In general, the Fe^{2+} concentrations reached are relatively low compared to those in the Calabrese and Porporato [11] simulations.

As far as carbon dynamics are concerned, the behaviour is fluctuating, alternating between upward and downward peaks. On the other hand, it can be seen that BM is a driver for Fe^{2+}, since peaks of BM correspond to peaks of Fe^{2+}.
ADD has an important influence on carbon in particular. Figure 15 shows the close connection between ADD and carbon for a variable s scenario.

In order to obtain higher Fe^{2+} values and to ensure that it is not continually decreased at minimum values, it is necessary to reduce oxidation by changing the k_{ox} parameter. Figure 16 shows the results of a simulation with a k_{ox} 1000 times smaller (k_{ox} = 0.0432 1/d). It can be seen that the dynamics of Fe^{2+} are at higher values and that it can accumulate at certain times. In the same figure, the great influence of ADD on the dynamics of Fe^{2+} can also be seen. Carbon and BM undergo minor changes by changing the k_{ox} and this is consistent with the fact that in the equations describing their dynamics the oxidation term does not appear.
The next steps are to develop the model for a multi-layered soil and to interpret the results by highlighting the similarities and differences between a model considering the soil as a single reactor and the same model developed for a soil divided into layers.

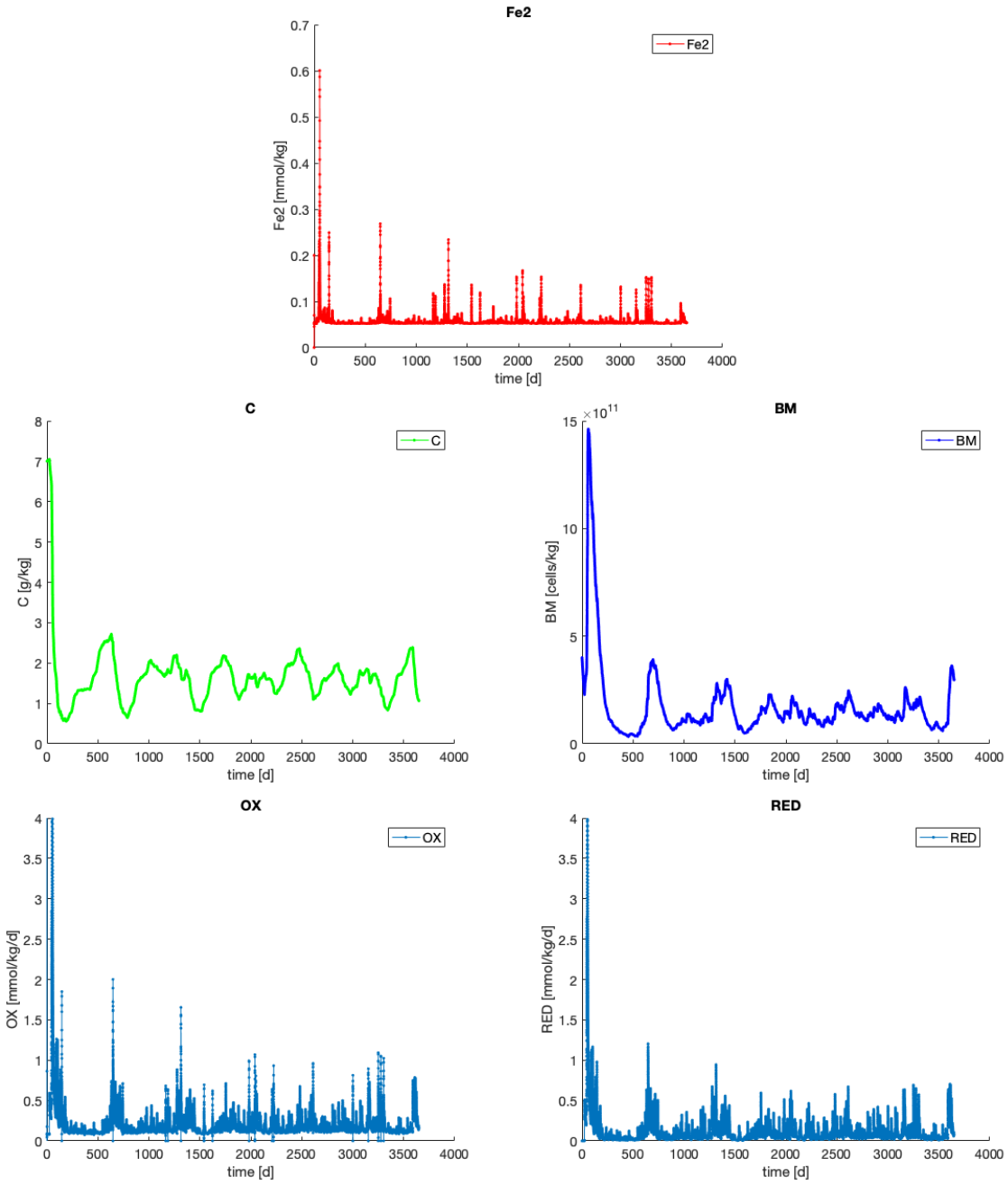

Figure 14: Scenario with s calculated from a stochastic rainfall, with ADD that varies monthly, presence of $L_{Fe^{2+}}$, soil depth= 0.75 m, without evapotranspiration. Top: time evolution of Fe^{2+} - Center left: time evolution of C - Center right: time evolution of BM - Bottom left: time evolution of OX - Bottom right: time evolution of RED.

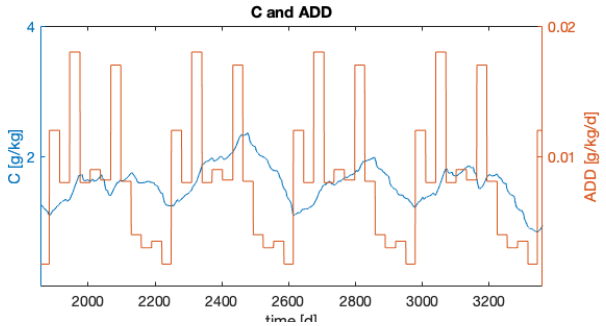

Figure 15: Scenario with s calculated from a stochastic rainfall, with ADD that varies monthly, presence of $L_{Fe^{2+}}$, soil depth= 0.75 m, without evapotranspiration. Effect of ADD on C.

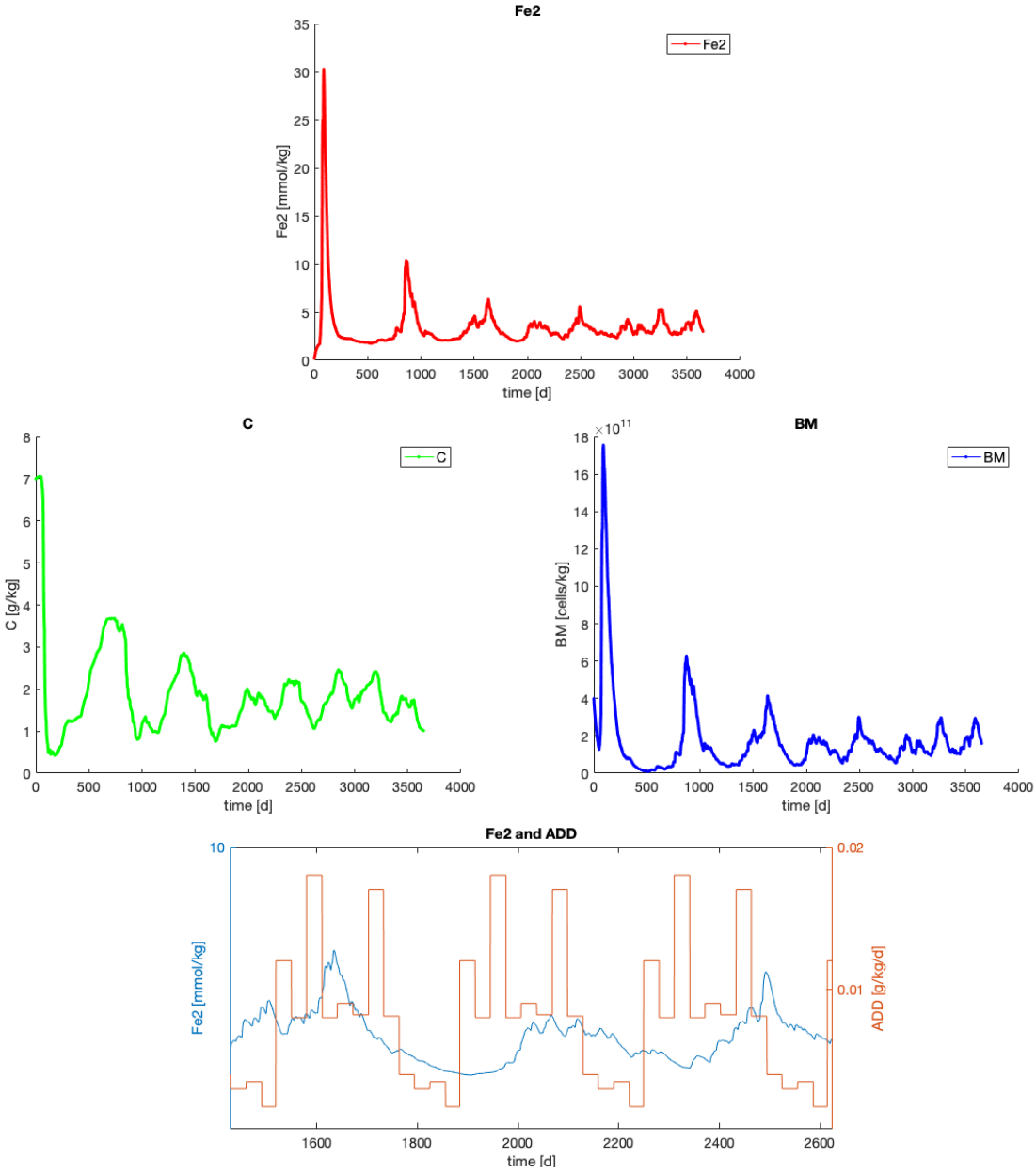

Figure 16: Scenario with s calculated from a stochastic rainfall, with k_ox 1000 times smaller, with ADD that varies monthly, presence of $L_{Fe^{2+}}$, soil depth= 0.75 m, without evapotranspiration. Top: time evolution of Fe^{2+} - Center left: time evolution of C - Center right: time evolution of BM - Bottom: Effect of ADD on Fe^{2+}.

6 Multi-layers soil

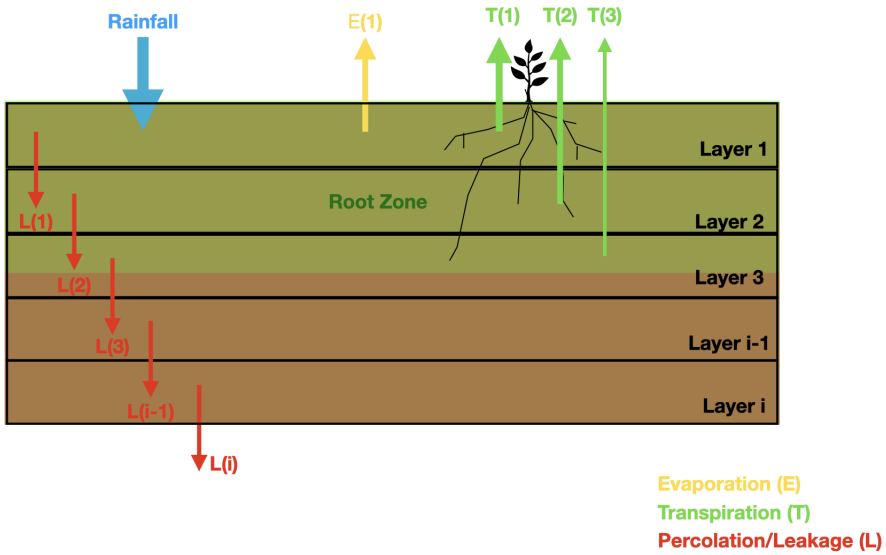

Figure 17: Schematic representation of multi-layer soil.

6.1 Methodology

This section discusses the model implementation for a soil modeled with multiple layers. The highlights and most important changes are clearly related to the transport and exchange that occurs between the different layers and related to how external inputs such as precipitation, litter fall and evapotranspiration affect the soil.

A first parameter that undergoes a change is the term of leakage, in fact in a soil modeled as a single reactor this was considered as a loss of water (L) that dragged with it a part of Fe^{2+} ($L_{Fe^{2+}}$), however in a multi-layered soil the leakage of the upper layer is transformed into a gain of water for the lower layer. Here then is a first very simplistic concept of fluxes between layers given by leakage. In addition, the rainfall will only act on the most superficial layer, so for the lower layers the main source of water is the leakage of the upper layers.

Another term that undergoes changes is the litter fall ADD, this is because it falls from above so only the upper layers are affected. A consequence of this change is the need to include a transport term (a flow between layers) for carbon to the lower layers. Similarly to ADD, evaporation and transpiration are also affected by multi-layered soil modeling because they occur with greater intensity in the shallowest part of the soil. These changes will be discussed in detail below.

6.2 Soil moisture dynamics reformulation

In the case of a modeled soil with several layers, the soil moisture equation remains the same for the first layer (the shallowest one) however for the layers below the equation of soil moisture dynamics changes. Rainfall only acts on the first layer, so from the second layer there will be no a rainfall term (J) but it will be replaced by a water flow from the layer above. This flow of water from the upper layer can be approximated to the loss of water that the upper layer experiences through leakage. Another term that will no longer be present is evaporation, which only occurs in the first layer, while transpiration will act differently depending on the depth. Transpiration and evaporation will be discussed in detail later.

Aware of the fact that a correct description of the hydrological process requires the full solution of the Richards equations, in this theoretical work the fluxes and loss of water are evaluated to satisfy the total mass balance equation: a sufficient condition that reflect the aims of this work in qualifying (rather than quantifying) the effect of fluxes exchange. A more rigorous approach from the point of view of the hydrodynamics will be adopted in the section 6.5.5 where the soil moisture dynamics is simulated by the software HYDRUS 1D [30], [31].

In this design the dynamics of the layers below the surface layer are governed by the following equation:

$$\eta \cdot D \cdot \frac{ds_i}{dt} = L_{i-1} - Q_i - T_i - L_i \tag{32}$$

where η is the soil porosity, D the layer thickness, Q the runoff and T the transpiration, while L_{i-1} represents the water added from the upper layer and L_i the water lost through percolation/leakage. In a multi-layer soil the leakage becomes a transport term, it remains a loss term for the layer considered but becomes an addition term for the lower layer. The fluxes between layers are therefore modelled simplistically using leakage. This transport term moves water from the upper layers to the lower layers, and in doing so also creates a transfer of Fe^{2+} due to the $L_{Fe^{2+}}$ parameter.

There is one particularity related to the term runoff Q to note. Because in the surface layer it can be considered that this amount of water runs off to the surface but in the lower layers this is not physically possible. However for the parameters used in this project this aspect can be neglected, this volume of water represents a very small part of the entire water balance. It would become a significant problem in the event of major rainfall or in the case of modelling a soil with very thin layers. Moreover, other terms such as capillary rise are not implemented in this model although they might take action in the case of a soil with several layers.

In this 1D lattice support, the general formulation of the reaction terms is the following:

$$\frac{d\Theta_i}{dt}_i = R_i + T_i + S_i \tag{33}$$

where Θ_i refers to ta generic species modelled at the layer i. The term R_i contains all the reaction terms while T and S represent transport and source or sink for the same specie at the same layer i. The spatial coupling between the layers is given then by the T transport which is promoted here to a fluxes Matrix by the following relation:

$$T_i = \sum_j M_{ij}\Theta_j \tag{34}$$

where the elements M_{ij} refers to the Φ_{ij} fluxes between the layer i and j (in general not necessarily adjacent). If a species is present only in the solid phase, its fluxes coefficient will be identically zero. As anticipated before, in this work, only adjacent layers can communicate as the leakage of the i layer is the positive flux of the $i+1$ assuming positive sign going along the depth. More complex and realistic Fluxes matrix can be considered representing an interesting future perspective.

6.3 Litter fall reformulation and carbon flux

In a multi-layer soil, litter fall (ADD) only occurs in the most superficial part of the modelled soil, in contrast to a soil modelled as a single reactor. This clearly creates an imbalance between the amount of carbon in the upper and lower layers. In order to make the "new model" more realistic and to have C substrate also in depth, it is necessary to introduce a carbon transport term from the upper layers to the lower layers via leakage, somewhat like the transport of Fe^{2+}.
Arbitrarily, the layers directly affected by the litter fall term are those with an mean depth of less than 20 cm, and all layers will be affected by the carbon transport term L_C,

$$L_C = \tau \cdot L(s) \cdot [C] = \tau \cdot L(s) \cdot \frac{C}{\eta \cdot s \cdot D} \tag{35}$$

which is proportional to the amount of carbon, C, and to the percolation rate, L(s). Moreover η is the soil porosity, D the layer thickness, s the soil moisture and τ ($= 0.08$, choosen value) is the fraction of organic carbon which is subjected to transport process.

In the case of the scenarios illustrated by figures 18, 20, 24 the soil is modelled with 10 layers of 10 cm thickness each, so the layers affected by litter fall are the two most superficial layers.

6.4 Evaporation and transpiration reformulation

With regard to evaporation and transpiration, in a multi-layer soil it is necessary to consider the differences that exist between the surface and deeper layers. The root zone of plants is considered to extend only into the upper layers, so the model has to be modified to differentiate between the layers, some of which are subject to transpiration while others are not. Similarly, evaporation can only be taken into account for the

superficial part of the soil. In order to do this, it is decided to apply evaporation only in the shallowest layer.
In the framework of multi-layer simulations with evapotranspiration, transpiration is modelled in such a way that it acts on the first 5 layers (50 cm) with decreasing intensity. The first two layers will both take a 30% portion of the transpiration, the third 20%, the fourth 15% and the fifth 5%. This is a rough assumption, what is important is to consider the differences between the layers and to maintain a realistic water balance.

6.5 Scenario simulation and discussion

6.5.1 Multi-layer scenario without evaporation and transpiration

Figure 18 illustrates the results of a simulation carried out for a multi-layer soil with 10 layers of 10 cm thickness each, but without considering evaporation and transpiration and therefore plant uptake. For this scenario the leakage exponent is set at $c = 3$, which is different from the value used in the first simulations (see table 1). The simulation is carried out for 10 years, Figure 18 shows an example of the evolution of soil moisture along the simulation, to make the plot readable a limited time interval was chosen and only 3 of the 10 layers of which the soil is composed. The numbering starts from the top and colorbar represents different layers, the first layer is number 1 and the last layer is number 10.

The litter fall that has been modelled as monthly variable as in the right part of figure 6 in the "new model" only affects layer 1 and layer 2 as they are the only ones located at a depth of less than 20 cm. All layers, however, are affected by a carbon transport term according to the equation 35.

Figure 18 shows the dynamics of Fe^{2+}, C and BM for three different layers. There is a difference between the behaviour of layer 2 and that of the other two layers illustrated. As far as iron Fe^{2+} is concerned, the difference between the layers is linked to the magnitude of the values and the trend remains similar in the different layers. In layer 2, Fe^{2+} is present in greater quantity and then decreases in depth.

On the contrary, for carbon and biomass, the difference is also at the level of the trend. While layer 2 shows a similar behaviour to that observed in the scenario of a soil as a single reactor (figure 14), the trend is completely different for the other two layers, layers 4 and 8.

In the case of carbon, for layers 4 and 8, a decrease in concentration is observed until close to zero and then an increasing trend is observed, which starts earlier for the shallower layer. This growth behaviour can be traced back to the carbon transport term (equation 35). Figure 19 shows the difference between the same layers simulated with and without transport terms (fluxes). It can be seen that without fluxes, the carbon concentrations of the lower layers are unable to rise again after falling (layer 4 and layer 8 curves without flows are superimposed). As far as layer 2 is concerned, it can be observed that without fluxes the trend is similar but shifted generally downwards, but towards the end of the simulation for some stretches also upwards.

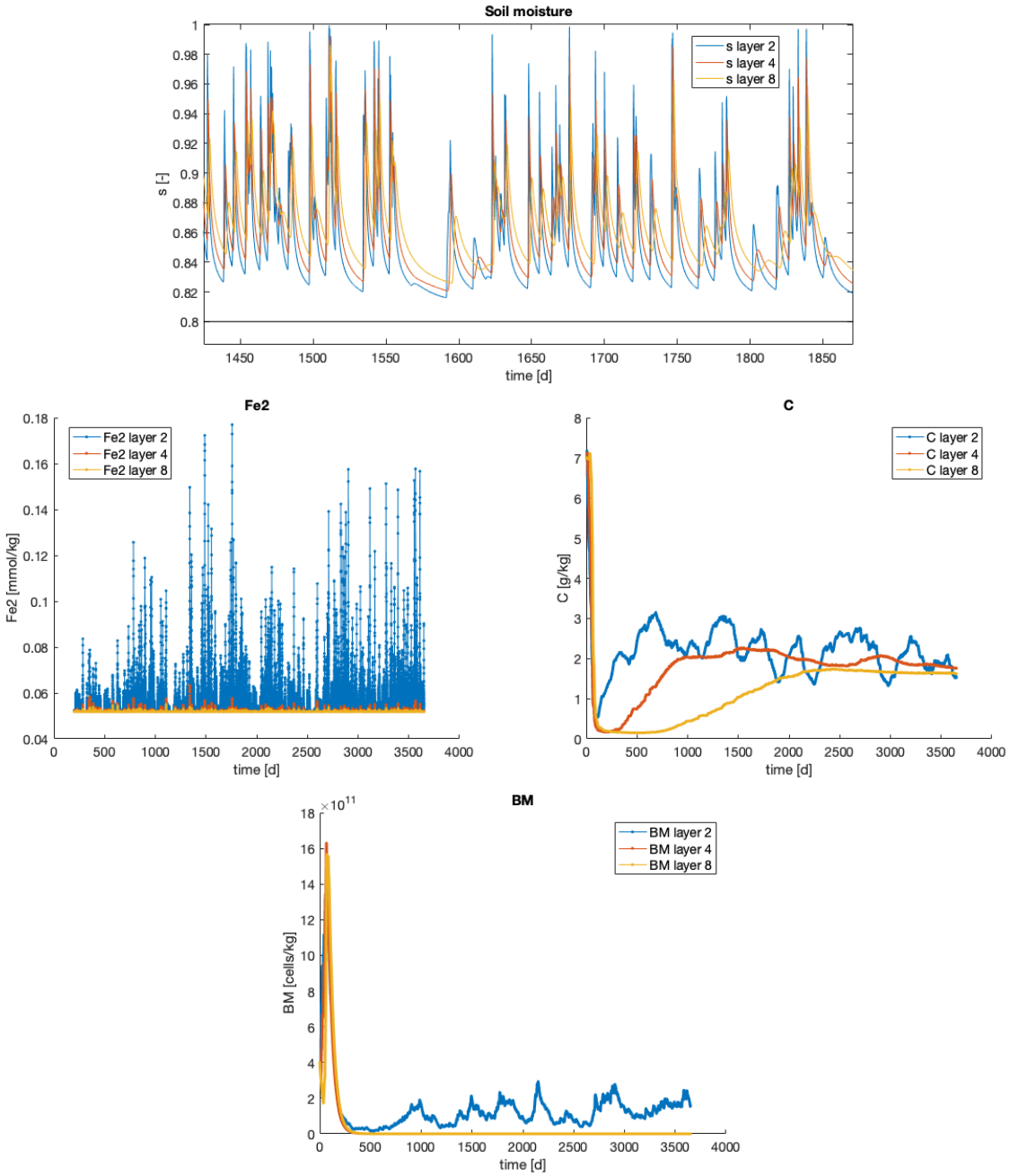

Figure 18: Multi-layer soil scenario with fluxes between layers, no evaporation and transpiration, ADD varying monthly (only layer 2). Colorbar represents three different layers out of the 10 simulated, all 10 cm thick, numbered from top to bottom. Top: extract of soil moisture evolution - Center left: time evolution Fe^{2+} - Center right: time evolution of C - Bottom: time evolution of BM

With regard to biomass, despite the downward carbon fluxes, the amount of biomass in the lower layers remains minimal and close to 0. On the other hand, for layer 2 the biomass has a dynamic characterised by peaks alternating with moments of relaxation.

From this scenario it can therefore be seen that ADD plays a key role in the activity of the layers. Layer 2 has a much higher activity than the lower layers, firstly because soil

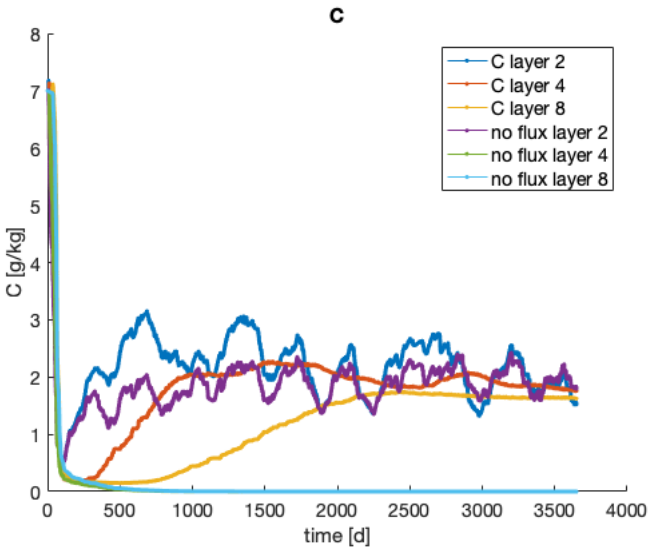

Figure 19: Comparison of carbon dynamic between multi-layer soil scenario with fluxes and the same scenario without incoming Fe^{2+} and C fluxes.

moisture reaches higher values, so the reduction is more important (due to less oxygen), but mainly because it has a more significant carbon source such as ADD. The carbon flux ensures the presence of carbon in the lower layers but this does not allow the BM and the production of Fe^{2+} to be raised, this suggests that carbon fluxes, as modelled, are not a full substitute for ADD.

6.5.2 Multi-layer scenario with evaporation and transpiration

In this scenario a seasonal evapotranspiration is considered, modelled by means of a sinusoidal curve. The effective evapotranspiration in this scenario corresponds to 54% of the precipitation and is divided between evaporation (32%) and transpiration (68%). As explained above, evaporation affects only the superficial layer while transpiration acts on the first 5 layers with different magnitude. Figure 22 shows the temporal evolution of transpiration for layers 1,2,4,5. The litter fall only affects the first two layers and a flow of carbon moves from the top to the bottom. For this scenario the leakage exponent is set at $c = 3$, which is different from the value used in the first simulations (see table 1).

An extract of the soil moisture evolution for different layers can be seen in figure 20. First of all, it can be seen that the deeper the layer, the more the soil moisture dynamics are attenuated. The first layer is the one with the greatest variations because it is directly affected by rainfall, evaporation and transpiration, while layer 8 is not directly affected by evapotranspiration and rainfall. Layer 8 is only affected by the flow of water coming from layer 7 and is therefore less subject to changes in soil moisture.
The dynamics of soil moisture and fluxes, which in this scenario are also influenced by evapotranspiration, have repercussions on the dynamics of the Fe^{2+}/Fe^{3+} redox couple, carbon and biomass. Figure 20 shows the differences between layers 1, 2, 4 and 8, chosen as a sample among the 10 simulated layers.
As far as Fe^{2+} is concerned, the greatest presence is observed in layer 2, mainly because soil moisture tends to decrease more in layer 1 (therefore more oxidation), while the underlying layers reach lower peaks of soil moisture (therefore an environment with

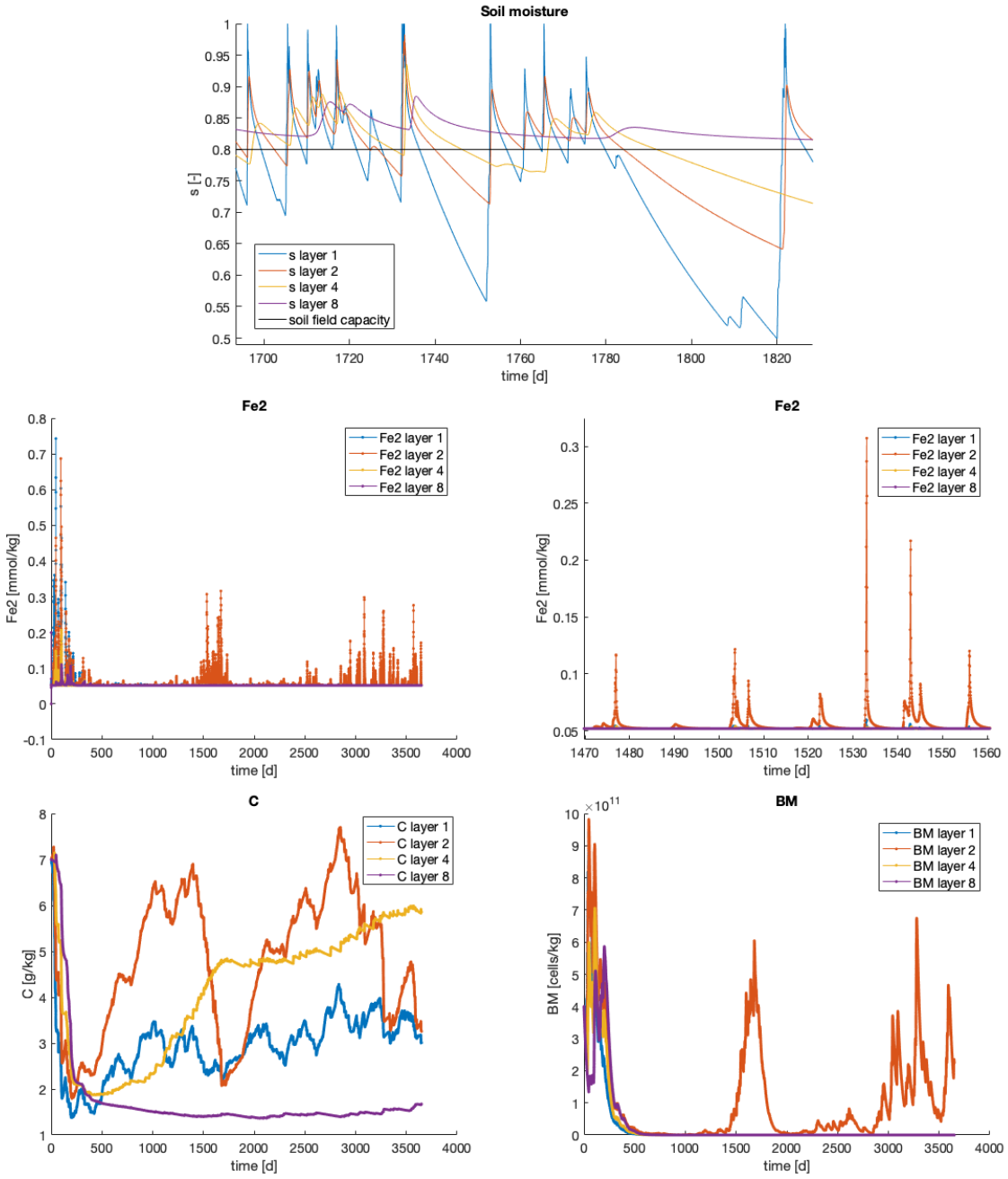

Figure 20: Multi-layer soil scenario with fluxes between layers, with evaporation and transpiration, ADD varying monthly (only layers 1 and 2). Colorbar represents four different layers out of the 10 simulated, all 10 cm thick, numbered from top to bottom. Top: extract of soil moisture evolution - Center left: time evolution Fe^{2+} - Center right: zoomed time evolution of iron Fe^{2+} - Bottom left: time evolution C - Bottom right: time evolution BM.

more oxygen, more favourable to oxidation) and furthermore they do not undergo the direct effect of litter fall, which, as explained, has an important role on the dynamics of Fe^{2+}. Similar behaviour is also observed for biomass, so again there is a strong link between biomass and Fe^{2+}, being BM is the population of bacteria that produces Fe^{2+}. For carbon, different trends are observed depending on the layers. In the first two layers, a dynamic characterised by continuous changes and alternating peaks and troughs is observed, although layer two is also the most active layer for carbon, with larger carbon

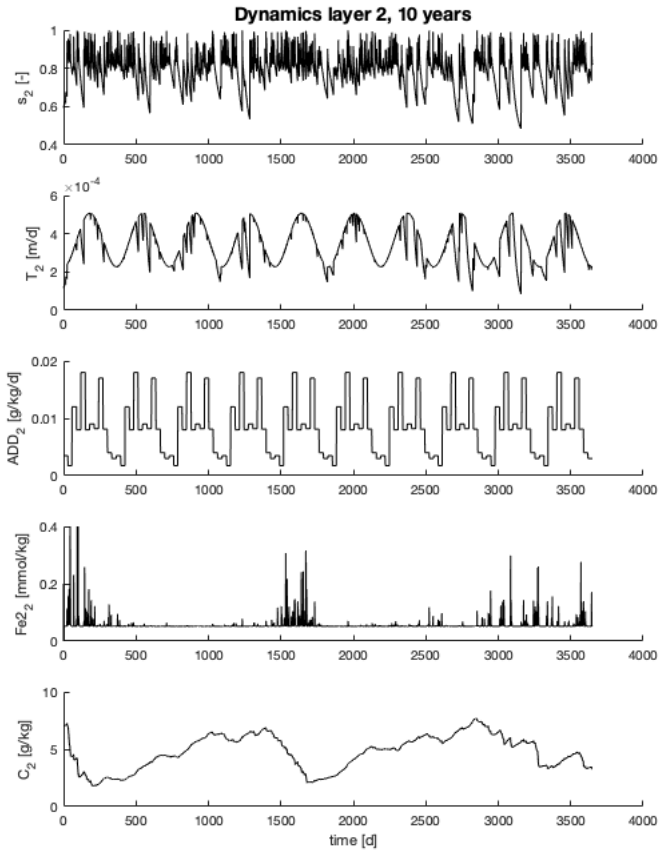

Figure 21: Dynamics layer 2 for a multi-layer soil scenario with fluxes between layers, with evaporation and transpiration, ADD varying monthly.

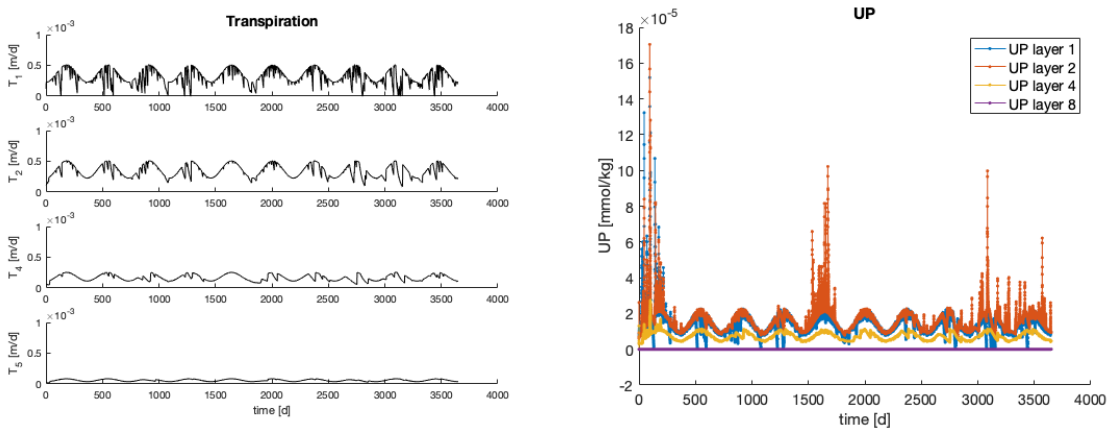

Figure 22: Transpiration (left) and plant uptake (right) for a multi-layer soil scenario with fluxes between layers, with evaporation and transpiration, ADD varying monthly.

values than the other layers. In layer four, which is an intermediate layer, a carbon fall is initially observed, but then a growth is observed, mainly due to the fluxes coming from the layers above. In layer 8, once the amount of carbon has fallen, it does not rise again for the duration of the simulation.

It may be interesting to look more closely at layer 2, where the amounts of carbon and Fe^{2+} are higher, in fact figure 21 shows these two concentrations, soil moisture, transpiration and litter fall, so it is possible to observe the reciprocal influence they may have on each other. Carbon and Fe^{2+} would appear to respond in opposite ways to ecohydrological conditions, in fact during periods when Fe^{2+} increases, carbon decreases, this is because carbon is consumed during reduction.

What can be emphasised from the results of this simulation is that while in a soil modelled as a single reactor the dynamics were varied and the same throughout the soil, in a multi-layer soil the dynamics of the variables depend on the location of the layer itself. There is therefore a zone where the activity of the Fe^{2+}/Fe^{3+} cycle and Fe-reducers (BM) is higher than in other zones. For the set of parameters used, and the way the initial model was changed, the zone of greatest activity is layer 2 where soil moisture levels reach sufficiently high peaks, creating sufficient anoxic conditions, which allow significant activity of Fe-reducers with consequent production of Fe^{2+}, and where soil moisture never falls too low, thus limiting the effect of oxidation. In addition, this layer 2 has a carbon source such as ADD which allows the concentrations of the variables to be increased, which is consistent with the findings of Calabrese and Porporato [11].

6.5.3 Multi-layer scenario with evaporation and transpiration and uniform ADD

In this scenario a seasonal evapotranspiration is considered, modelled by means of a sinusoidal curve. The effective evapotranspiration in this scenario corresponds to 54% of the precipitation and is divided between evaporation (32%) and transpiration (68%). As explained above, evaporation affects only the superficial layer while transpiration acts on the first 5 layers with different magnitude.
Figure 23 illustrates the results of the simulation carried out for a multi-layer soil composed of 10 layers of 10 cm thickness each, considering an ADD that acts on all layers and not just the first two. For this scenario the leakage exponent is set at $c = 3$, which is different from the value used in the first simulations (see table 1).
Physically, the ADD would only fall in the first layers, but in this scenario it is taken into account for all layers, as if there was a uniform distribution of this carbon source in the soil.

In this case, it can be seen that, due to the presence of a carbon source (ADD), all layers have a marked and varied activity. The result is a more homogeneous soil in terms of species presence, even if the activation and activity of the layers has shifted over time. At some times it is the upper layers that have the most activity, at other times it is the lower layers. This is mainly driven by soil moisture, and to a small extent also by fluxes between layers. In fact the variations of soil moisture are smoothed at depth, in layer 1 both the highest and lowest values of soil moisture are observed (due to the external inputs, as rainfall, evaporation and transpiration) while in layer 8 the soil moisture is within a smaller range and shows a smoothed dynamics. This behaviour due to the external inputs acting differently on the different layers results in layer 1 being more saturated at some times and layer 8 being more saturated at other times, implying that the highest soil activity is located at different depths depending on when the soil is being observed.

The result that the ADD is decisive within the model is repeated thanks to this sce-

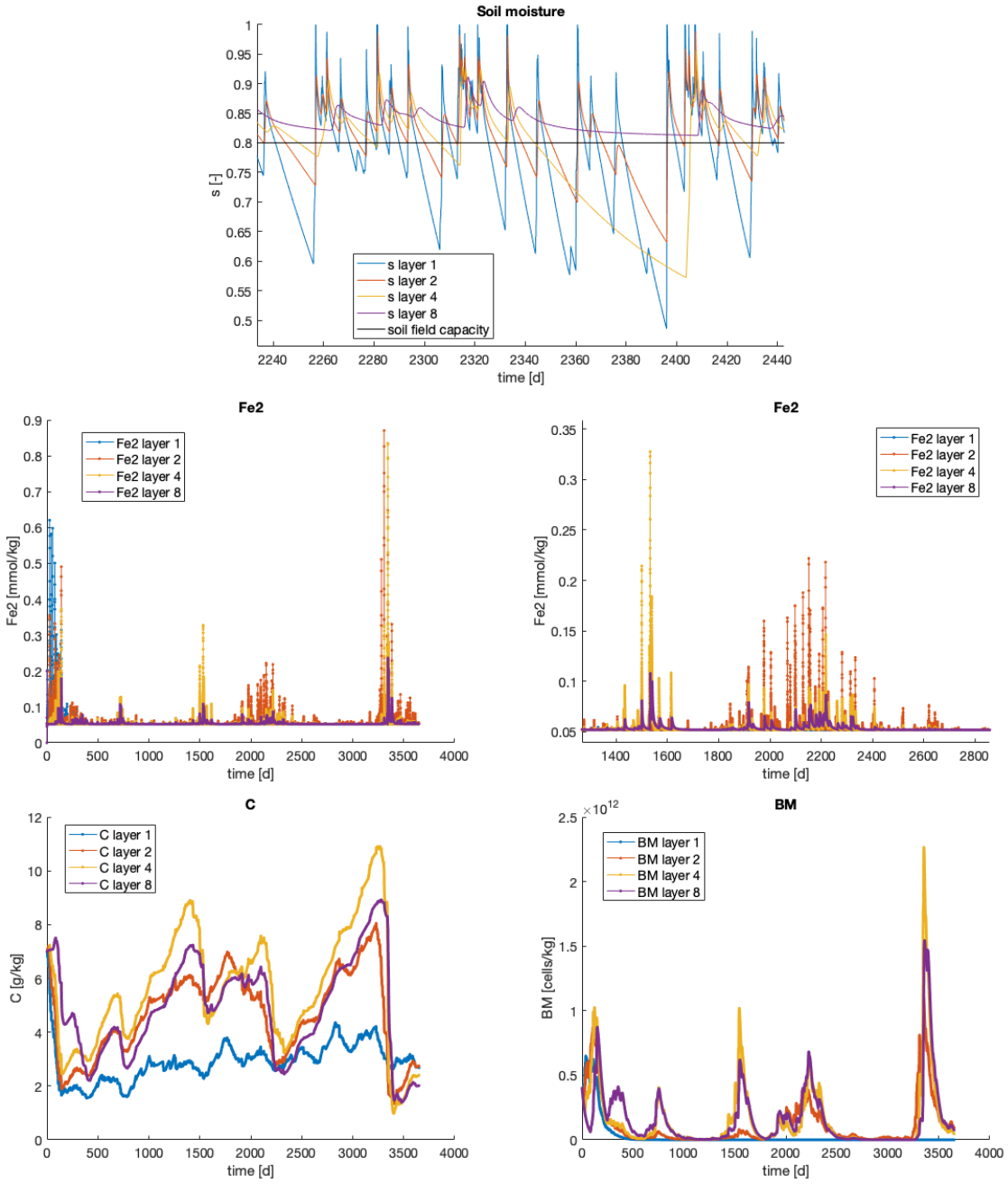

Figure 23: Multi-layer soil scenario with fluxes between layers, and considering seasonal evaporation and transpiration, soil moisture varying, ADD varying monthly and uniform through the soil. Colorbar represents four different layers out of the 10 simulated, all 10 cm thick, numbered from top to bottom. Top: extract of soil moisture evolution - Center left: time evolution Fe^{2+} - Center right: zoomed time evolution of iron Fe^{2+} - Bottom left: time evolution C - Bottom right: time evolution BM.

nario, in fact all layers have a marked activity. Layer 1 is the only exception, suffering the effect of evaporation and transpiration for different periods soil moisture falls significantly below soil field capacity levels, making oxidation more marked (due to the increased presence of oxygen) and as the model is formulated, these periods of strong oxidation significantly decrease BM and Fe^{2+}.

6.5.4 Limited oxidation multi-layer scenario

In this scenario the k_{ox} is 1000 times smaller (k_{ox}=0.0432 1/d). In the previous scenarios one can see the difficulty of Fe^{2+} to accumulate, as soon as the soil moisture dropped below a certain threshold the oxidation was sufficient to decrease Fe^{2+} almost to a minimum. Therefore the k_{ox} is reduced in this scenario to simulate a soil limited in oxidation. Scenario 6.5.2 has the same parameters except for a larger k_{ox}. The ADD acts on the first two layers and evapotranspiration is present.

It can be seen that in this scenario, on the contrary to the scenario 6.5.2 all layers are active on relatively high values, although in a different way.
As far as Fe^{2+} is concerned, it can be seen that layer 1 has lower concentrations, because being subject to evaporation and transpiration the soil moisture is often at lower values than in the other layers, so oxidation is greater. In the other layers, Fe^{2+} is at higher values and a very varied dynamic can be observed, which cannot be attributed only to variations in soil moisture and differences caused by litter fall. In this case the fluxes between the layers have an important impact on the dynamics of Fe^{2+} . The carbon dynamics remain similar but the biomass grows even in the deepest layers, which was not the case with a greater k_{ox}.

With a smaller k_{ox}, which results in a limited oxidation scenario, Fe^{2+} has more varied dynamics and is able to accumulate for some periods unlike before. Fluxes assume a key role in the dynamics of Fe^{2+} and BM, replacing the importance of ADD in the "activation" of the lower layers. In this scenario the dynamics of the variables respond to changes in soil moisture given by the hydrological components of the model and to changes in litter fall regime, however, the fluxes between the different layers are responsible for behaviours that cannot be explained by considering only soil moisture and litter fall. Figure 25 shows the difference in the dynamics of the four study layers if the inflows fluxes are not taken into account. For the first layer the two curves are perfectly superimposed since the most superficial layer is not subject to fluxes from above. It can be seen that the dynamics are very different for the lower layers, in particular for layer 8, peaks are reached that would not be possible without the contribution of Fe^{2+} fluxes from the upper layers. In this scenario, Fe^{2+} can be produced in one layer and then transported to another.

Therefore, according to the parameters used, the fluxes between the layers have more or less importance for the dynamics of the variables. In such a scenario it becomes more difficult to predict the temporal and spatial evolution of the variables without taking into account all the components of the model. In the case of a field experiment or in the laboratory a new calibration of the parameters can be decisive for the prediction and description of the spatial and temporal patterns.

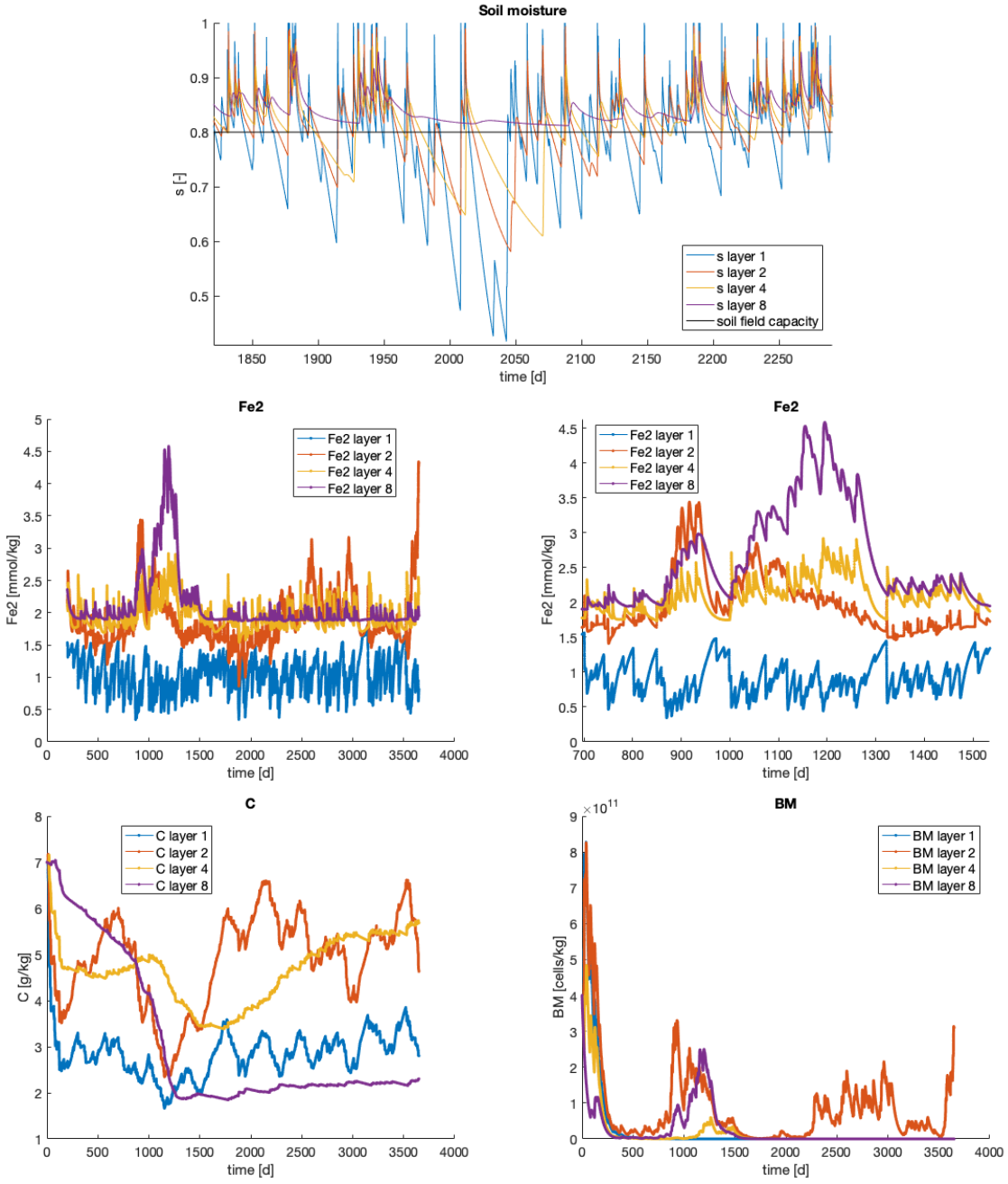

Figure 24: Multi-layer soil scenario, with k_{ox} 1000 times smaller, with fluxes between layers, with evaporation and transpiration, ADD varying monthly (only layers 1 and 2). Colorbar represents four different layers out of the 10 simulated, all 10 cm thick, numbered from top to bottom. Top: extract of soil moisture evolution - Center left: time evolution Fe^{2+} - Center right: zoomed time evolution of iron Fe^{2+} - Bottom left: time evolution C - Bottom right: time evolution BM.

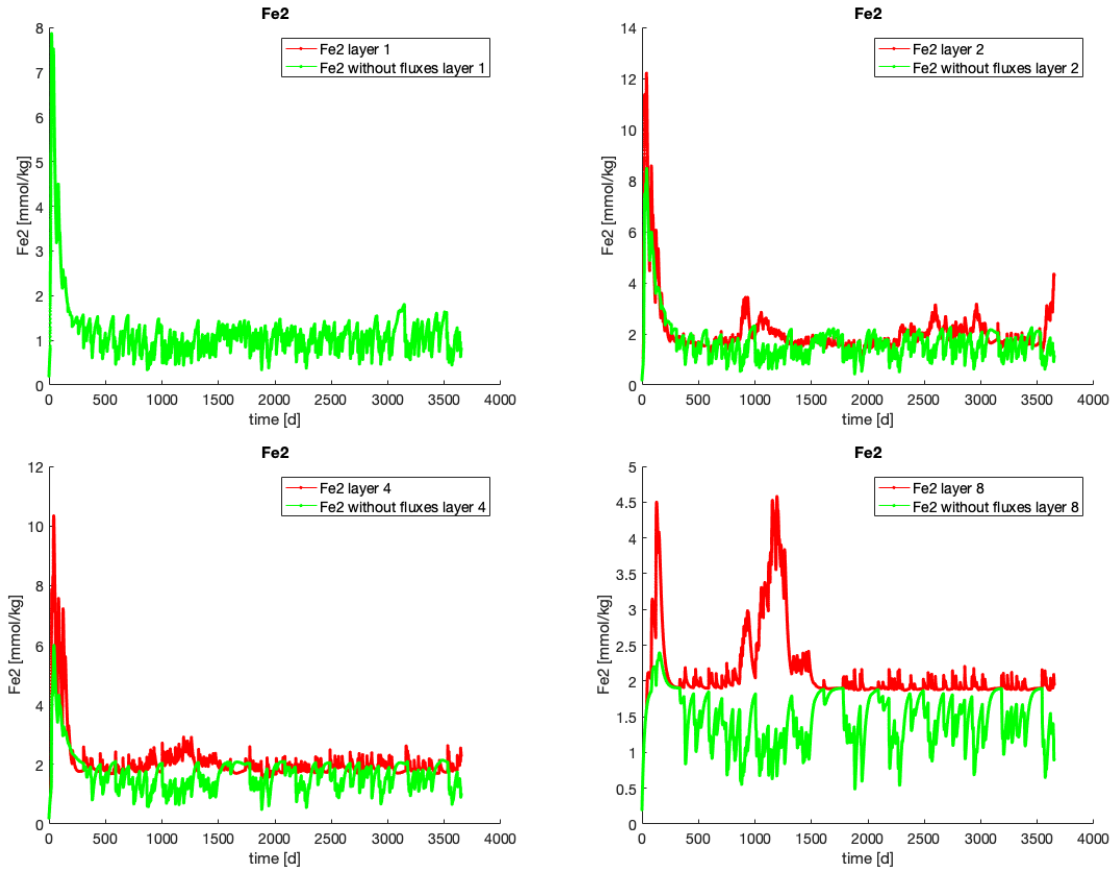

Figure 25: Comparison of Fe^{2+} dynamic between multi-layer soil scenario, with k_{ox} 1000 times smaller, with fluxes between layers, with evaporation and transpiration, ADD varying monthly (only layers 1 and 2) and the same scenario without incoming fluxes. Top left: layer 1 - Top right: layer 2 - Bottom left: layer 4 - Bottom right: layer 8.

6.5.5 Multi-layer scenario with HYDRUS dataset

In this case the dataset is generated with the help of HYDRUS software. HYDRUS allows to generate a set of soil moisture and fluxes for a multi-layered soil. This is extremely interesting in the context of this project as it allows for a sequence of fluxes between layers to which the model implemented for a multi-layered soil can be applied.

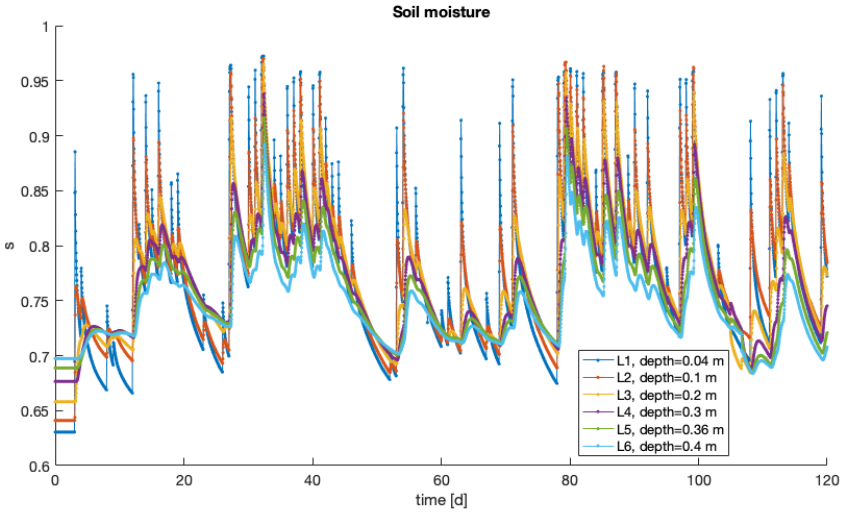

Figure 26: Soil moisture series for HYDRUS dataset scenario without evapotranspiration and with ADD uniform through the soil. Colorbar represents different layers.

The results of the simulation with the soil moisture series in figure 26 are shown in figures 27 and 28. In contrast to the simulations previously presented, the following one is based on a dataset covering a smaller period of time, namely 120 days and the portion of the soil considered is smaller (0.4 m).

In this case, the ADD is constant and equal for all layers, as if the soil had been mixed before the experiment and evapotranspiration is not considered. First of all, it should be noted that soil moisture is often below the soil field capacity ($s_{fc} = 0.8$) where reduction does not take place because f(s) is equal to 0 and where oxidation is at full capacity because g(s) is equal to 1. Only occasionally due to some peaks does soil moisture exceed the soil field capacity, at which time reduction starts and oxidation is limited.

These soil moisture behaviours are reflected in the Fe^{2+} dynamics in the form of peaks and depending on the depth (i.e. the layer considered), the peaks are of different intensity. The deeper the layer and the lower the peaks, the more superficial layers being directly touched by the rain reach higher peaks of soil moisture, the quantity of oxygen is less due to the water present in the soil and therefore the oxidation decreases and the reduction increases. In the lower layers this phenomenon is attenuated as the soil moisture reaches lower values. Not considering the evapotranspiration the only external input is the rainfall and that is why the dynamics of the soil moisture is very similar among all layers if not for an attenuation of the variations going down in depth.

Figure 28 shows the soil profile and the values of Fe^{2+}, C, BM and soil moisture as a function of depth during one of the soil moisture peak and at the end of the same soil moisture peak (end of the decreasing edge). It can be seen that Fe^{2+} is mainly affected

by a spatial trend change, while C and BM maintain the same trend during and after the peak. During the peak, Fe^{2+} is higher in the surface layers, decreases going deeper until it is constant between the last layers. After the peak, the difference between the layers is smaller, but it can be seen that initially the amount of Fe^{2+} increases as you go deeper (up to 10 cm), and then starts to decrease as you go deeper. After the peak, the amount of Fe^{2+} at a depth of 4cm is less than that observed at 10cm and 20cm. Fe^{2+} reflects the behaviour of soil moisture, which also increases during the peak as it goes deeper, but after the peak it is higher in the middle depths than at the surface.

Concerning C and BM, it is interesting to note that the two variables behave in opposite and mirror-like ways, their behaviour is mainly driven by soil moisture and to a lesser extent by fluxes.

Figure 29 shows the simulation results for the same soil moisture but with a k_{ox} 50 times smaller and an Fe_r 3 times larger. This change has a direct effect on the oxidation rate and indirectly on the other variables. The greatest differences are observed in the dynamics of Fe^{2+} and Fe^{3+}, with Fe^{2+} taking on larger values and the smearing within the Fe^{3+} dynamics becoming more significant and visible.

Furthermore, if the "Fe^{2+} vs s" curve of the two simulations is compared, it can be seen that between the initial case (figure 27) and the case with a smaller oxidation rate (figure 29), the relationship between Fe^{2+} and s follows two different trends. In the initial case the "Fe^{2+} vs s" curve shows an almost exponential relationship (figure 27) for which given a value of s it is possible to estimate the value of Fe^{2+}, while in the case of a smaller oxidation rate a very different form of the "Fe^{2+} vs s" curve is observed for which, within a single cycle, given a value of s there are two very different values of Fe^{2+} (figure 29).

In this model oxidation prevails over reduction, Fe^{2+} does not accumulate this even by limiting the oxidation rate. Comparing these two "HYDRUS" scenarios to the other multi-layers scenario, despite a much shorter simulation duration, it can seen much less diversity between the dynamics of the different layers, because there are no the external inputs of evaporation, transpiration and there is an equal ADD for all layers. This means that, for the parameters used in this scenario, the fluxes between layers alone can not break the pattern given by soil moisture, which is the main driver of the system in this case.

Before to conclude this section, it is important to mention at this point that the effect of internal fluxes that activate bottom layers on different timing can be analytically handled by the same instability analysis performed in chapter 4. The spatial formulation of the soil as a sequence of layers can be generalised by including spatial heterogeneity, gas exchange and preferential flow paths, suggesting that a network support instead of a 1D lattice could represent a better realisation of the support. It has been proved in [32] [33] that, in this context, the instability analysis can be easily extended to the case of reaction dispersion system hosted on directed networks. For this purpose, the full knowledge of the elements of the flux matrix M_{ij}, (most of the time available only with a tracer experiment [34]), is necessary as its eigenvalues drives the condition to let the instability to evolve.

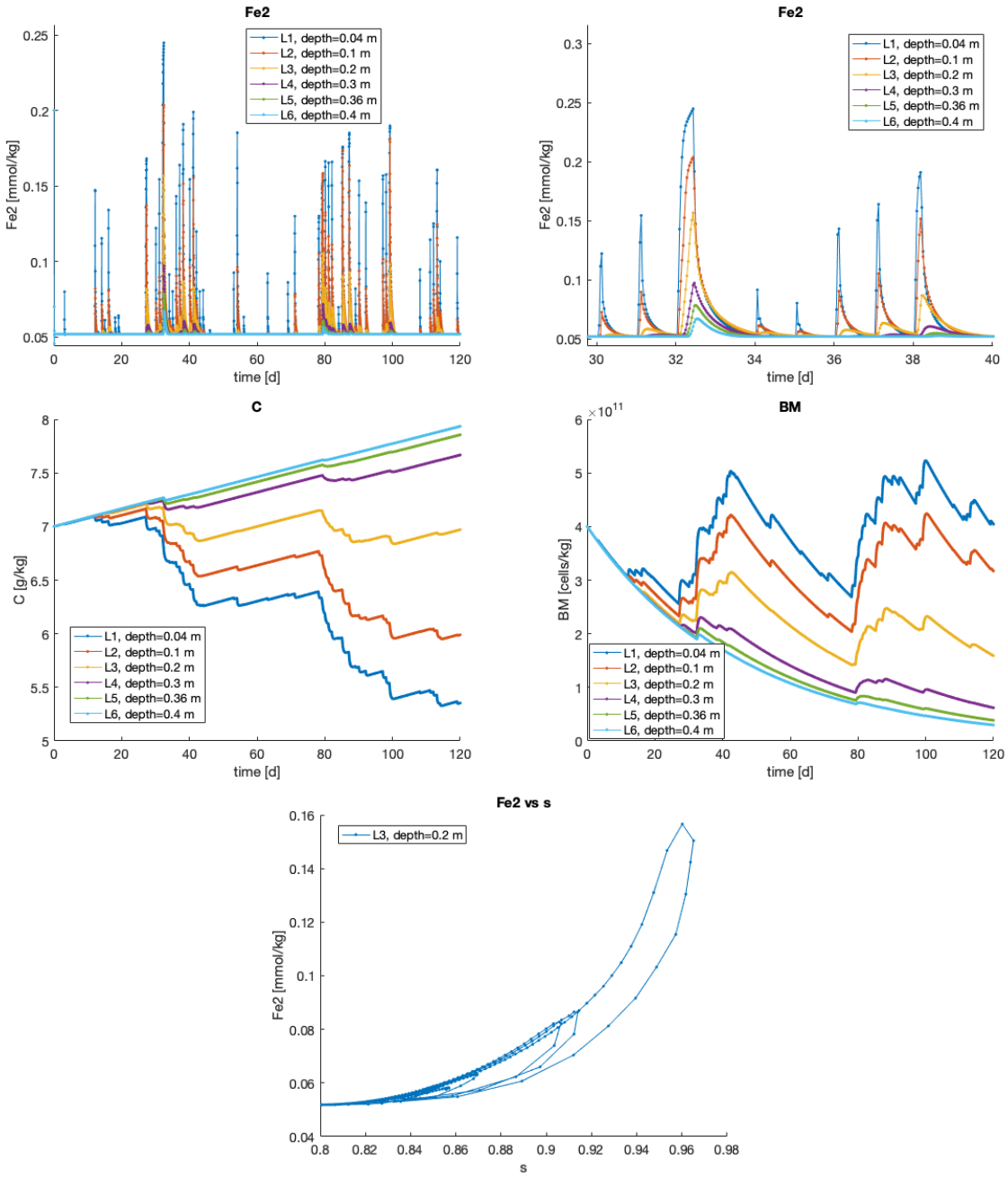

Figure 27: HYDRUS dataset scenario, with ADD = 0.1 [g/kg/d] constant in all layers, flux between layers from the HYDRUS dataset. Colorbar represents different layers. Top left: time evolution of Fe^{2+} - Top right: zoomed time evolution of Fe^{2+} - Center left: time evolution of C - Center right: time evolution of BM - Bottom: extract of "Fe^{2+} vs s" curve for layer 3.

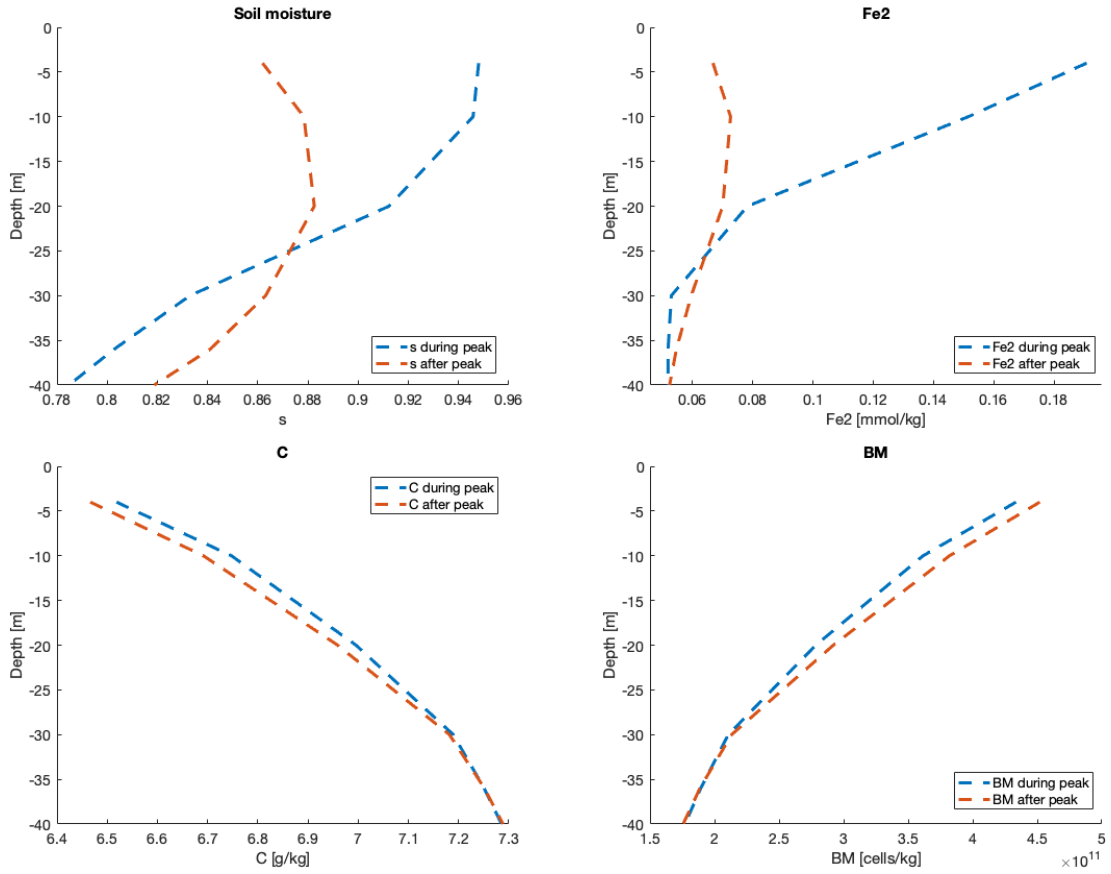

Figure 28: HYDRUS dataset scenario, with ADD = 0.1 [g/kg/d] constant in all layers, flux between layers from the HYDRUS dataset. Colorbar represents different time (durign peak, after peak). Top left: spatial evolution of s - Top right: spatial evolution Fe^{2+} - Bottom left: spatial evolution of C - Bottom right: spatial evolution of BM.

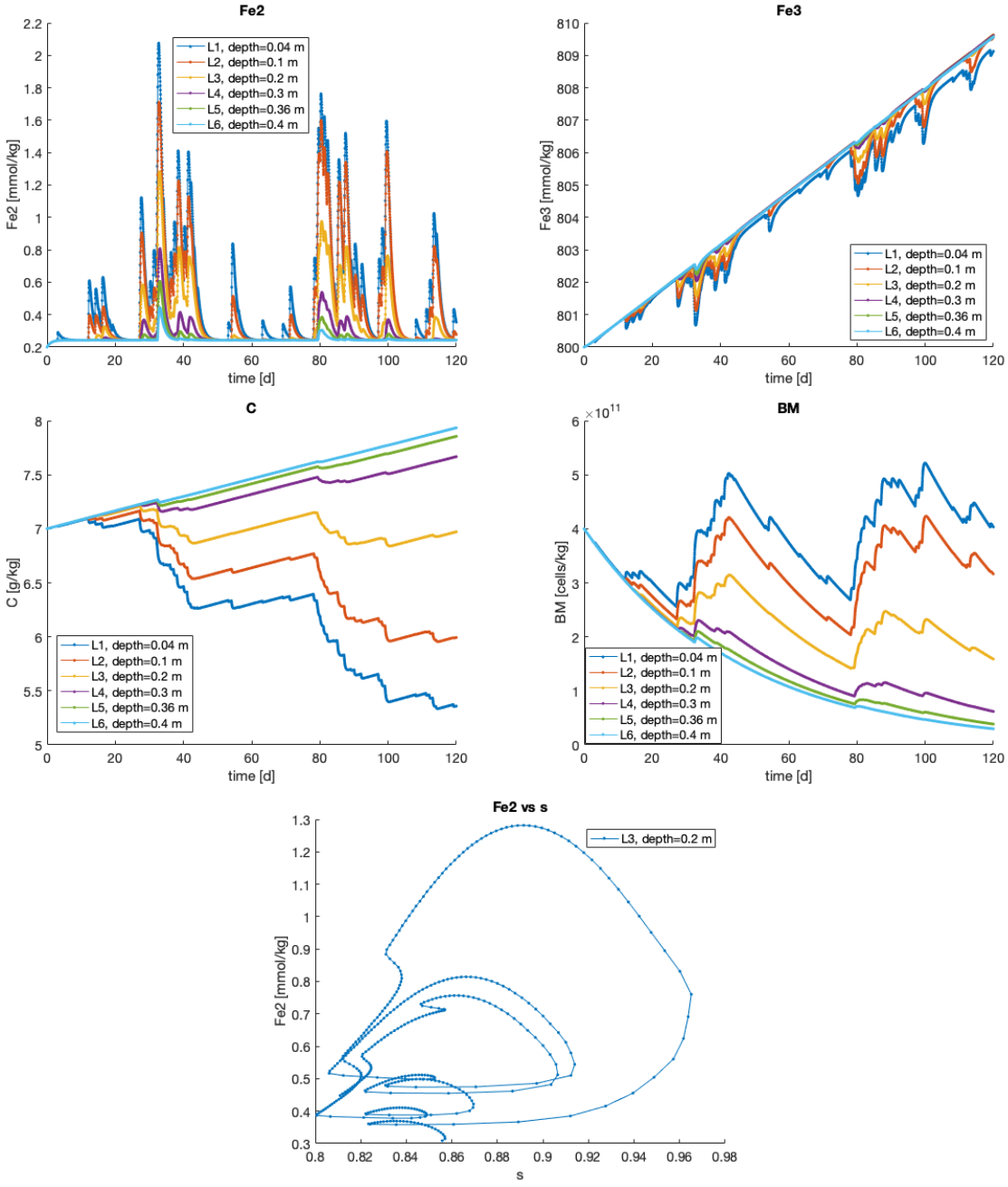

Figure 29: HYDRUS dataset scenario, with k_{0X} 50 times smaller and $Fe2_r$ 3 times greater, with $ADD = 0.1$ [g/kg/d] constant in all layers, flux between layers from the HYDRUS dataset. Colorbar represents different layers. Top left: time evolution of Fe^{2+} - Top right: time evolution of Fe^{3+} - Center left: time evolution of C - Center right: time evolution of BM - Bottom: extract of "Fe^{2+} vs s" curve for layer 3.

7 Redox potential dynamics

In the previous sections the flexibility of the model were exploited by exploring possible outputs that correspond to scenarios where different inputs of rainfall/drainage regime and carbon supply were imposed. This kind of "boundary conditions" can be plausibly applied to either experimental field and laboratory conditions and the spatial and temporal evolution of the concentrations that can be obtained from the model can provide a guide in interpreting data already collected or in planning new experiments or field campaigns.

As anticipated in the introduction, the interplaying between climate change, rainfall regime, soil respiration and microbial activity is as intimate as it is complex to study and even more complicated to predict. However, when measures of the redox potential are feasible and available in specific and well controlled environmental conditions, they can be useful in identifying which is the leading reaction occurring in a specific space-time location of the soil.

Redox potential measures the tendency of a specific portion of the soil to donate (or accept) electrons through the embedding environment. Practically, it describes the stress to which a given microbial community is subjected and gives information on which type of metabolism is promoted and which is inhibited.

For a couple of two species involved in a redox reaction:

$$\mathbf{Ox} + ne^{-} \leftrightarrow \mathbf{Red} \tag{36}$$

where **Ox** and **Red** are the oxidized and reduced species respectively and n is the number of electrons e, exchanged, the redox potential is computed by the Nerst equation:

$$Eh(t) = Eh^{0} - \frac{KT}{ne} \ln \frac{[\mathbf{Ox(t)}]}{[\mathbf{Red(t)}]} \tag{37}$$

where K is the Faraday constant, T the temperature and Eh^{0} the standard electrode potential referred to that specific reaction when measured in a standard solution of molecular hydrogen. The squared brakets [.] are the "activity" of the two species, a quantity that can be directly related to the concentration itself of the two species. It is clear that its time evolution is governed by the time evolution of the two redox species. Indeed, under the assumption that in a specific region of the soil the occurring leading reaction

is the dissimilatory reduction, it is possible to take advantage of the model developed to describe which redox potential rate change is expected.

Interesting results can be drawn from the data set of a column experiment performed by master's student Ivan Retti under the supervision of Prof. Rizlan Bernier-Latmani at EPFL, available for the ECHO group.

7.1 Column experiment

The experiment involved a lysimeter filled with soil where weekly cycles of rainfall and drainage were applied. The system was equipped of: a shower on the top where rainwater was irrigated, four soil moisture sensors placed at different depths and six redox probes placed at 6 different depths. The system was drained by applying a negative pressure from the bottom at pressure of $\simeq$ -60 KPa. Samples of collected water from the bottom have been analysed to monitor the increasing concentration of iron(II), nitrate, nitrite, sulfide and ammonium involved in the different microbial metabolism. The cycles alternate periods of saturated condition (7 day) to fast drainage phases (3.5 days). The aim of the experiment was to monitor the fluctuations of redox potential and relate them to soil moisture fluctuation and saturation level. Combining the redox readers with the samples collected at the bottom, they tried to evaluate the impact of soil moisture dynamics on the evolution of the microbial community and, more precisely, to identify which was the dominant respiration occurring.

The microbial community has been previously doped by initially saturating the soil column with rainwater with high concentration of dissolved organic carbon (precisely, cellobiose in concentration specified by [35], [36]), and the experiment was thought to be divided in two macro phases: the first four cycles without any carbon supply while for the last four cycles, 20 cm of litter has been added on top of the first layer. It is important to notice that after that carbon was mended on the top, the concentration of Fe2+ sampled in the out flowing water started to increase significantly.

For the reason above, the data collected and shown in figure 30 and 31 represent a valid data set of a space-time series of soil moisture and redox potential measured at the same time.

By neglecting the slow negative drift during the saturated period, soil moisture's sensor in figure 30 showed a similar behavior at all the depths. Thus, at this step, we can refer to the system as a single reactors. While for the redox series shown in figure 31, a common pattern is evident and further three different trends can be easily recognised. Indeed, all the sensors are sensitive to the alternation oxic/anoxic condition which means that both oxidation phase (where redox potential drops up) and reductant phase (where redox potential drops down) are almost instantaneously triggered by soil moisture fluctuations. The different trends, instead, are summarised as follow:

- Sensors in the middle layers oscillate in a synchronized manner and within the same range of redox potential.
- The sensor at the bottom is the first that decay to lower values during a saturation period.

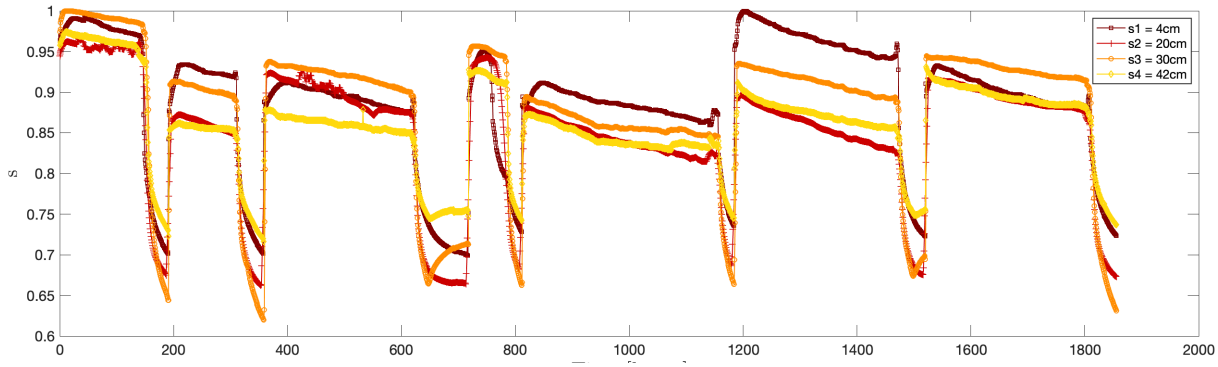

Figure 30: soil moisture from Ivan experiment: time series of soil moisture sensor: the color map goes from the darkest (top layer) to the lightest (bottom layer). During the saturated period, the lysimeter was closed on the top and the bottom to prevent water loss. However, a negative drift is evident but the saturation level still remained above its soil field capacity estimated around 0.8

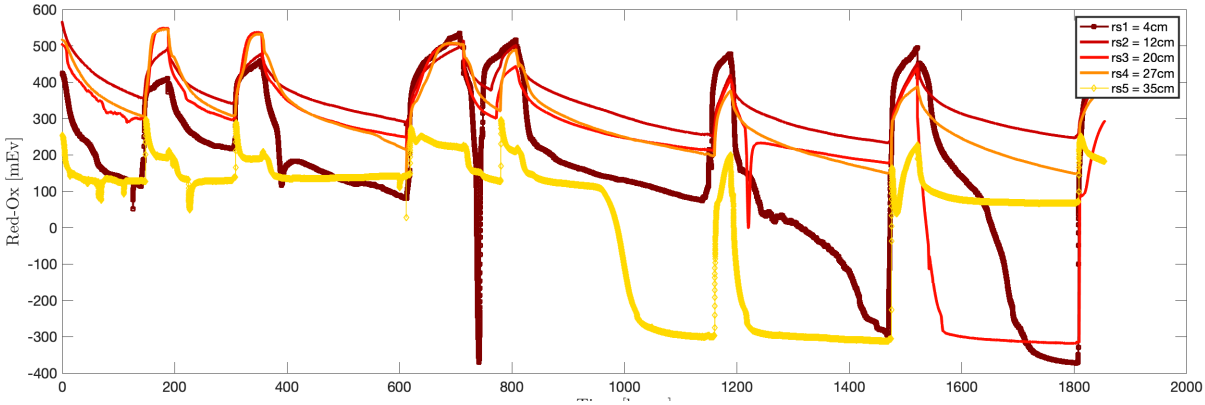

Figure 31: Redox time series from Ivan experiment: the color map goes from the darkest (top layer) to the lightest (bottom layer). There is a clear one-to-one relation between soil moisture profile and redox changes before the first 800 hours. Then bottom layer is then the first more affected by anaerobic respiration and the top layer is the second one.

- The sensor at the top is the second one that decay to lower value during a saturation period.

7.2 Theoretical prediction of redox rate change

By choosing, thus, the series of the sensor nr. 3 at 30 cm depth and smoothed it to remove aberrant value prior to use as input of the model, the rate in change of the simulated redox potential will be compared to the one obtained from the data. Performing the time derivative of eq. (37) it is possible then to compare the numerical derivative of the redox time series of sensor 5 with the term:

$$\dot{Eh}(t) \propto \left(\frac{\left[\dot{Fe^{3+}}\right]}{[Fe^{3+}]} - \frac{\left[\dot{Fe^{2+}}\right]}{[Fe^{2+}]} \right) \rightarrow \gamma \left(\frac{RED}{\alpha_1} - \frac{OX}{\alpha_2} \right) \tag{38}$$

where the terms RED and OX are the one defined in the model by eq. (1) and the coefficient γ, α_1 and α_2 are calibration parameters at this stage.

The comparison between the result obtained from the model by eq. (38) and the layer 5 and 6 are shown in figure 32.

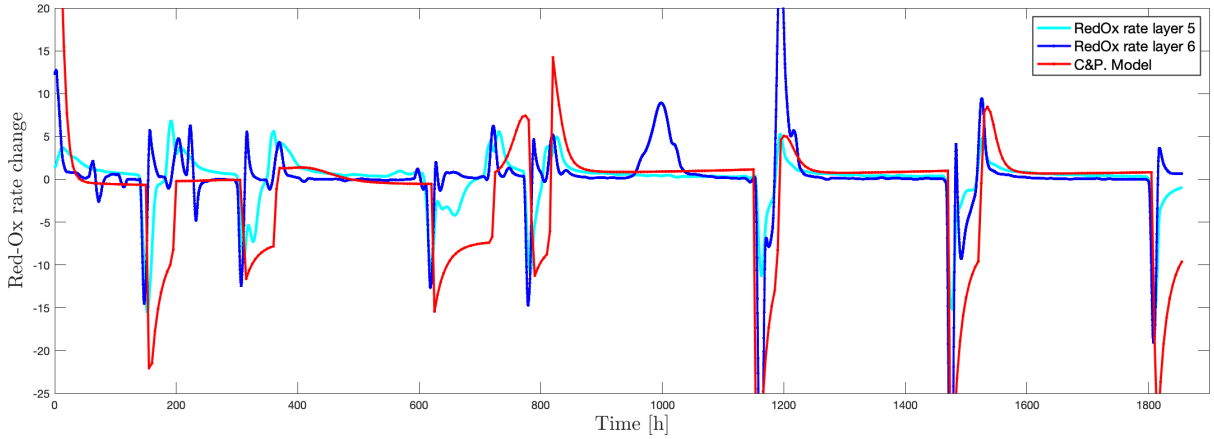

Figure 32: redox rate change: comparison between experimental data of layer 5 (cyan), 6 (blue) and the model (red) line.

For this comparison, a value for k_{ox} 1000 times smaller has been chosen as already noticed in the previous sections since the original value corresponded to a too fast oxidising environment where practically no Fe^{2+} can be accumulated.

The agreement between the model and the time derivative of redox probes readings for the two chose layers highlights the pros and cons of this strategy.

The model seems to properly catch the right timing of the major positive-negative peaks in the redox rate change. This is not surprising as these peaks reflect the rapid change between oxic/anoxic conditions that are well described by the modulating functions $f(s)$ and $g(s)$ that promotes/inhibits the reduction/oxidation cycles due to low/high oxygen availability. However, the model is not able to describe the series of smaller and more frequent peaks and it cannot catch the slowly negative jump (corresponding to a positive drop in the time derivative plot) that the bottom layer experienced at the time around 1000 hours during a period of fully saturated conditions.

The reason is obvious and it lies in the fact that the importance of Fe^{3+} reduction is overestimated. Indeed this is a general drawback of the model as it is absolutely not contextualised in a more complex redox framework where prior to the Fe^{3+} consumption, other electron acceptors (O_2 and NO_3) are previously consumed [3]. All these species are involved in coupled redox reactions and they are affected by the same alternance of oxic/anoxic condition. This type of issue can be handled by extending the proposed model to include the other alternative metabolism with a similar scheme of coupled ODEs.

Reminding then that the soil moisture profiles for all the layers exhibit a similar behavior, the question why exactly the bottom layer is the first experiencing this jump is the

hardest to answer, especially if we consider how the experiment has been carried out. The soil has been mixed prior to filling the column to reduce initial spatial heterogeneity in the microbial community. The irrigation has been always performed from the top as the new carbon supply after the fourth cycle has been added on top of the first layer. However, the last and deepest layer was the first that has been activated. The most plausible explanation is that this is a mark of the effects of the inner fluxes and the existence of preferential flow paths by which a non-negligible fraction of initially irrigated dissolved organic carbon fastly reaches the bottom layer (and sediment also) doping microbial community enough to consume O2 and nitrate faster than the other layers.

Quantifying the existence of such preferential flow paths, although not sensibly revealed by soil moisture sensors, and how they impact solute transport requires a full control of the fluxes and the transport process occurring along the depth of the lysimeter which has been theoretically investigated in this work and represent an interesting future perspective from the point of view of applicability to real experimental data.

8 Conclusion

The model for the "Dissimilatory" Fe2-Fe3 reduction presented by Calabrese and Porporato has been formulated and qualitatively studied by means of an instability analysis conducted on the Carbon/Biomass pair in its "single layer" formulation that consider soil as a single bioreactor. The results showed that the system can exhibit inner fluctuations even for constant environmental conditions, that are triggered by the nested nonlinear behaviour of the two species. The stationary solutions depend on soil moisture and litter fall (ADD) dynamics, which also play a role in the type of convergence or non-convergence of the variables towards them.

Soil moisture proves to be an important driver within the dynamics and this is taken into account through modulating functions representing the amount of oxygen within the soil that promotes/inhibits the oxidation and the reduction rate. ADD also plays a key role, and its seasonal/monthly evolution is reflected within the dynamics of Fe^{2+}, C and BM.

The model has been then adapted to simulate a multi-layer soil by considering explicit spatial effects on the dynamics. Here, rainfall is supposed to affect only on the first layer, same as evapotranspiration that acts more on the surface part of the soil and litter fall, a source of carbon, is only present in the upper layers. The novelty of this work is then represented by the implementation of fluxes that occur between layers.

The multi-layer soil simulations carried out showed that for the set of parameters used, different soil depth reactive on different timing and all of them are strongly influenced by soil moisture and litter fall.

Precisely, the hydrological components such as rainfall and evapotranspiration are reflected in the dynamics of soil moisture. Here, the most reactive soil areas are those where soil moisture experience high peaks, most of the time close to full saturation. Layers with periods of low soil moisture level, such as the most superficial layer, are characterized by a strong oxidation and do not allow the Fe^{2+} to reach high values and accumulate as it happens in the most active layers.

Layers with a less varied soil moisture dynamics instead, such as deeper layers, fail to activate due to an environment not sufficiently reducing and especially due to the lack of litter fall. By homogenizing the space carbon source availability, lower layers also have a much stronger dynamic and the soil becomes active in all its zones at different times with different but comparable intensities. When considering only rain, without considering evapotranspiration and with an equal ADD throughout the soil, the dynamics respond essentially to soil moisture variations.

Scenario	Description
No evapotranspiration, ADD first 2 layer, k_{ox} greater	Soil moisture similar in all layers, dynamics more active in layers with ADD. ADD is the main driver.
Yes evapotranspiration, ADD first 2 layer, k_{ox} greater	Soil moisture dynamics attenuated by going deep, increased activity where there is ADD and soil moisture is high (layer 2). One part of the soil is very active (layer 2), the rest is not very active.
Yes evapotranspiration, ADD uniform, k_{ox} greater	All soil is active, but at different times depending on the different soil moisture dynamics.
Yes evapotranspiration, ADD first 2 layer, k_{ox} smaller	The whole soil is active. Fluxes are important, dynamics cannot be explained based on soil moisture dynamics and ADD alone.
No evapotranspiration, ADD uniform, k_{ox} greater	The main driver is soil moisture which is similar in all layers with a slight attenuation going deeper. Fluxes do not break the pattern given by soil moisture.

Table 3: Multi-layer scenarios summary

Interesting, by decreasing the oxidation rate parameter, k_{ox}, it is possible to observe how the flows between the layers assume importance and become determinants in order to describe the spatial and temporal evolution of the variables. In fact, some behaviours cannot be explained only with the help of the soil moisture series and the ADD regime contrary to what predicted and expected in the single layer formulation. The overall behaviors for the multilayer's version is summarised in table 3.

Finally, we took advantage of the simulations by feeding the model with a real time series of soil moisture levels measured at different depths in a lysimeter experiment to predict the time evolution of Fe^{2+}, Fe^{3+}, carbon and biomass concentrations. The simulated redox reaction can be related to the rate of change of redox potential and the output of the model has been compared to the time series of redox readings measured at different depths during the same experiments. The comparison between the data and the model highlights the power of the model in catching the rapid switch between oxic/anoxic conditions but showed also its weakness in simplifying the complex dynamics occurring in the soil in conditions of constant saturation level. However, the data of the redox profile showed different patterns for different depths in a counterintuitive manner. This discrepancy can be handled with the "multilayer" formulation of the model after a proper description of the internal fluxes occurring into the lysimeter representing an interesting future perspective of the current work.

References

[1] Thomas G. Huntington. Evidence for intensification of the global water cycle: Review and synthesis. *Journal of Hydrology*, 319(1):83–95, 2006.

[2] Ove Hoegh-Guldberg, Daniela Jacob, Michael Taylor, Marco Bindi, Sally Brown, Ines Camilloni, Arona Diedhiou, Riyanti Djalante, Kristie L. Ebi, Francois Engelbrecht, Joel Guiot, Yasuaki Hijioka, Shagun Mehrotra, Antony Payne, Sonia I. Seneviratne, Adelle Thomas, Rachel F. Warren, Guangsheng Zhou, and Petra Tschakert. *Impacts of 1.5^{o}C global warming on natural and human systems.* IPCC, 2018.

[3] Paula Rodríguez-Escales, Carme Barba, Xavier Sanchez-Vila, Diederik Jacques, and Albert Folch. Coupling flow, heat, and reactive transport modeling to reproduce in situ redox potential evolution: Application to an infiltration pond. *Environmental Science & Technology*, 54(19):12092–12101, 2020. PMID: 32897067.

[4] Stahl D. Madigan M., Martinko J. and Clark D. *Brock: Biology of Microorganisms.* Thirteenth Edition, Pearson, 2010.

[5] Daniel Uteau, Silke Hafner, Sebastian Kouso Pagenkemper, Stephan Peth, Guido L. B. Wiesenberg, Yakov Kuzyakov, and Rainer Horn. Oxygen and redox potential gradients in the rhizosphere of alfalfa grown on a loamy soil. *Journal of Plant Nutrition and Soil Science*, 178(2):278–287, 2015.

[6] Jianwu Tang, Mark A. Bradford, Joanna Carey, Thomas W. Crowther, Megan B. Machmuller, Jacqueline E. Mohan, and Katherine Todd-Brown. Chapter 8 - temperature sensitivity of soil carbon. In Jacqueline E. Mohan, editor, *Ecosystem Consequences of Soil Warming*, pages 175–208. Academic Press, 2019.

[7] Stefano Manzoni and Amilcare Porporato. A theoretical analysis of nonlinearities and feedbacks in soil carbon and nitrogen cycles. *Soil Biology and Biochemistry*, 39(7):1542–1556, 2007.

[8] Andrew J. Guswa, M. A. Celia, and I. Rodriguez-Iturbe. Models of soil moisture dynamics in ecohydrology: A comparative study. *Water Resources Research*, 38(9):5–1–5–15, 2002.

[9] N. Tufkenji, J. A. Redman, and M. Elimelech. Interpeting deposition patterns of microbial particles in laboratory-scale column experiments. *Environ. Sci. Technol.*, 37:616–623, 2003.

[10] M. Elimelech, Xi Jia, J. Gregory, and R. A. Williams. *Particle Deposition and Aggregation - Measurement, Modeling and Simulation.* Butterworth Heinemann, 1995.

[11] Salvatore Calabrese and Amilcare Porporato. Impact of ecohydrological fluctuations on iron-redox cycling. *Soil Biology and Biochemistry*, 133:188–195, 2019.

[12] F. Laio, A. Porporato, L. Ridolfi, and I. Rodriguez-Iturbe. Plants in water-controlled ecosystems: active role in hydrologic processes and response to water stress: Ii. probabilistic soil moisture dynamics. *Advances in Water Resources*, 24(7):707–723, 2001.

[13] D R Lovley. Dissimilatory fe(iii) and mn(iv) reduction. *Microbiological reviews*, 55(2):259–287, 06 1991.

[14] Derek Lovley. *Dissimilatory Fe(III)- and Mn(IV)-Reducing Prokaryotes*, pages 287–308. Springer Berlin Heidelberg, Berlin, Heidelberg, 2013.

[15] Derek R. Lovley and Elizabeth J. P. Phillips. Organic matter mineralization with reduction of ferric iron in anaerobic sediments. *Applied and Environmental Microbiology*, 51(4):683–689, 1986.

[16] C. Colombo, G. Palumbo, J. He, R. Pinton, and S. Cesco. Review on iron availability in soil: interaction of fe minerals, plants, and microbes. *Journal of Soils and Sediments*, 2014.

[17] Aaron Thompson, Oliver A. Chadwick, Denis G. Rancourt, and Jon Chorover. Iron-oxide crystallinity increases during soil redox oscillations. *Geochimica et Cosmochimica Acta*, 70(7):1710–1727, 2006.

[18] Nyle C Brady, Ray R Weil, and Ray R Weil. *The nature and properties of soils*, volume 13. Prentice hall Upper Saddle River, NJ, 2008.

[19] Karrie A. Weber. Microorganisms pumping iron: anaerobic microbial iron oxidation and reduction. *Nature Reviews Microbiology*, 2006.

[20] W. H. Patrick Jr. and A. Jugsujinda. Sequential reduction and oxidation of inorganic nitrogen, manganese, and iron in flooded soil. *Soil Science Society of America Journal*, 56(4):1071–1073, 1992.

[21] P. D'Odorico, L. Ridolfi, A. Porporato, and I. Rodriguez-Iturbe. Preferential states of seasonal soil moisture: The impact of climate fluctuations. *Water Resources Research*, 36(8):2209–2219, 2000.

[22] P. D'Odorico, L. Ridolfi, A. Porporato, and I. Rodriguez-Iturbe. Preferential states of seasonal soil moisture: The impact of climate fluctuations. *Water Resources Research*, 36(8):2209–2219, 2000. _eprint: https://agupubs.onlinelibrary.wiley.com/doi/pdf/10.1029/2000WR900103.

[23] Ignacio Rodriguez-Iturbe, Gregor K. Vogel, Riccardo Rigon, Dara Entekhabi, Fabio Castelli, and Andrea Rinaldo. On the spatial organization of soil moisture fields. *Geophysical Research Letters*, 22(20):2757–2760, 1995.

[24] Eric E. Roden. Geochemical and microbiological controls on dissimilatory iron reduction. *Comptes Rendus Geoscience*, 338(6):456–467, 2006. Les hydroxydes ferrosiques, les rouilles vertes et la fougérite dans le cycle biogéochimique du fer.

[25] James D. Murray. *Mathematical Biology. I. An Introduction.* Springer-Verlag New York, 2002.

[26] I. Rodriguez-Iturbe, A. Porporato, L. Ridolfi, V. Isham, and D. R. Coxi. Probabilistic modelling of water balance at a point: the role of climate, soil and vegetation. *Proceedings of the Royal Society of London. Series A: Mathematical, Physical and Engineering Sciences*, 455(1990):3789–3805, 1999.

[27] Steven H. Strogatz. *Nonlinear Dynamics and Chaos with Student Solutions Manual.* CRC Press, NJ, 1994.

[28] S. Manzoni, A. Porporato, P. D'Odorico, F. Laio, and I. Rodriguez-Iturbe. Soil nutrient cycles as a nonlinear dynamical system. *Nonlinear Processes in Geophysics*, 11(5/6):589–598, 2004.

[29] Brian Ginn, Christof Meile, Jared Wilmoth, Yuanzhi Tang, and Aaron Thompson. Rapid iron reduction rates are stimulated by high-amplitude redox fluctuations in a tropical forest soil. *Environmental Science & Technology*, 51(6):3250–3259, 2017. PMID: 28244747.

[30] JIRKA ŠIMŮNEK. Analytical and numerical modeling of physical and chemical processes in the vadose zone. In Adolf Ebel and Teimuraz Davitashvili, editors, *Air, Water and Soil Quality Modelling for Risk and Impact Assessment*, pages 221–233, Dordrecht, 2007. Springer Netherlands.

[31] Jirka Simunek, Jiri, Hirotaka Saito, Masaru Sakai, and Martinus Van Genuchten. *The HYDRUS-1D Software Package for Simulating the One-Dimensional Movement of Water, Heat, and Multiple Solutes in Variably-Saturated Media.* 01 2008.

[32] Silvia Contemori, Francesca Di Patti, Duccio Fanelli, and Filippo Miele. Multiple-scale theory of topology-driven patterns on directed networks. *Phys. Rev. E*, 93:032317, Mar 2016.

[33] Hiroya Nakao. Turing patterns in network-organized activator–inhibitor systems. *Nature Physics*, 6:544–550, 2010.

[34] Pierre Queloz, Luca Carraro, Paolo Benettin, Gianluca Botter, Andrea Rinaldo, and Enrico Bertuzzo. Transport of fluorobenzoate tracers in a vegetated hydrologic control volume: 2. theoretical inferences and modeling. *Water Resources Research*, 51(4):14. 2793–2806, 2015.

[35] Phan Van T.H., Rizlan Bernier-Latmani, Delphine Tisserand, Manon Frutschi, Antoine Gehin, Raoul-Marie Couture, Fabrizio Bardelli, Pierre Le Pape, and Laurent Charlet. As release under the microbial sulfate reduction during redox oscillations in the upper mekong delta aquifers, vietnam: A mechanistic study. *Science of the Total Environment*, 663:718–730, 2019.

[36] Stefanie Schellenberger, Harold L. Drake, and Steffen Kolb. Functionally redundant cellobiose-degrading soil bacteria respond differentially to oxygen. *Applied and Environmental Microbiology*, 77(17):6043–6048, 2011.